

Quark-universal $U(1)$ breaking scalar at the LHC

Lorin Armbruster^{*}, Bogdan A. Dobrescu[◇], Felix Yu^{*}

^{*} *PRISMA+ Cluster of Excellence & Mainz Institute for Theoretical Physics,
Johannes Gutenberg University, 55099 Mainz, Germany*

[◇] *Particle Theory Department, Fermilab, Batavia, IL 60510, USA*

June 6, 2025

Abstract

If the quarks or leptons are charged under a new $U(1)$ gauge symmetry, then besides a Z' boson there must exist at least one new boson whose decay products include Standard Model particles. In the case of a minimal symmetry breaking sector, that new boson is a scalar ϕ that couples to the Z' boson as well as to the new fermions required to cancel the $U(1)$ gauge anomalies. The scalar may be produced at the Large Hadron Collider (LHC) in association with a Z' boson, or through Z' boson fusion, while its decays are typically into four jets or two photons. We analyze in detail the case where the Z' boson is leptophobic, and all the quarks have the same charge under the new $U(1)$. If ϕ mixes with the Standard Model Higgs boson, then the new scalar can also be produced via gluon fusion, and the discovery mode is likely to be a diphoton resonance.

Contents

1	Introduction	2
2	Quark-universal $U(1)_B$ gauge symmetry	4
2.1	Scalar responsible for $U(1)_B$ breaking and anomalon masses	5
2.2	Scalar production at hadron colliders	9
2.3	Branching fractions of the scalar ϕ	10
2.4	LHC signals of the ϕ scalar	16
2.4.1	Low $M_\phi/M_{Z'}$	16
2.4.2	High $M_\phi/M_{Z'}$	17
2.4.3	Intermediate $M_\phi/M_{Z'}$	18
3	Effects of Higgs mixing	18
3.1	Higgs decay $h^0 \rightarrow \varphi\varphi^{(*)}$ or resonant diHiggs process $\varphi \rightarrow h^0h^0$	20
3.2	Mixing effects on the 125 GeV Higgs-like scalar h^0 and φ	22
3.2.1	Production modes for φ	23
3.2.2	Decay modes of φ	23
4	Conclusions	30
	References	32

1 Introduction

In the Standard Model (SM), the Higgs field plays a central role as the source of electroweak symmetry breaking via its vacuum expectation value (vev), generating the masses of the electroweak gauge bosons and the charged SM fermions. In $U(1)$ gauge extensions of the SM, such as gauging a linear combination of baryon and lepton global number [1–15], generic charge choices require new fermions to cancel the gauge anomalies (“anomalons”). In addition, introducing a scalar field Φ that spontaneously breaks the $U(1)$ gauge symmetry affords a renormalizable description to generate the Z' mass as well as anomalon masses, avoiding phenomenological constraints from measurements of the 125 GeV Higgs boson [13, 14].

In this paper we study the properties and Large Hadron Collider (LHC) phenomenol-

ogy of the new scalar particle (ϕ , the radial degree of freedom of Φ) responsible for the Z' mass. Generically, ϕ production at the LHC predominantly occurs in association with a Z' boson, and through Z' -mediated vector boson fusion. We focus on the predictions of the minimal renormalizable $U(1)_B$ model, in which the Z' boson has flavor-universal couplings to the SM quarks, and the anomalous are color singlets but carry chiral electroweak and $U(1)_B$ charges [8, 10, 11]. Since the anomalous are not colored, the new scalar would not be produced through gluon fusion at the LHC except via a model-dependent mixing with the 125 GeV Higgs boson. This contrasts other work on the Higgs sector of gauged baryon number symmetry [16], which relied on a colored anomalon content.

On the decay side, the scalar associated with new $U(1)$ chiral symmetries decays to Z' pairs as a result of spontaneous symmetry breaking, as well as to pairs of $U(1)$ chiral fermions proportional to Yukawa couplings. If decays to fermions are kinematically disallowed, the anomalous mediate loop-induced decays of ϕ to any and all gauge bosons under which the anomalous are charged. These loop interactions are nondecoupling as a result of Higgs low-energy theorems, and provide a characteristic pattern of Higgs decays in chiral theories compared to theories where fermions also have vectorlike masses [17, 18]. In our study of a quark-universal $U(1)_B$ gauge symmetry with anomalous carrying SM electroweak charges, the ϕ scalar acquires 1-loop couplings to pairs of gauge bosons, most importantly $\gamma\gamma$, $Z'\gamma$, $Z\gamma$, $Z'Z$, ZZ , and WW .

Mass mixing between ϕ and the SM Higgs boson leads to an important interplay between the phenomenology of the Higgs boson and of the new physical scalar, denoted by φ . For the quark-universal $U(1)_B$ model, since ϕ has intrinsic decays to $\gamma\gamma$, $Z\gamma$, ZZ , and WW , its effects on the 125 GeV SM-like Higgs boson are not solely captured by the typical interpretation of a mixing angle with a SM gauge singlet scalar. This pattern of coupling modifications on the observed 125 GeV Higgs boson offers a new benchmark to expand the interpretation power of the current suite of coupling measurements by the ATLAS and CMS experiments [19–21]. Crucially, the imprints of the SM Higgs phenomenology on the new scalar dictate interference effects sensitive to the mixing angle parameter and the individual chiral symmetries seen by the unmixed Higgses. A related work that studies the anomalon content from the point of view of dark matter is [22].

The outline of this paper is as follows. In Section 2, we analyze the quark-universal $U(1)_B$ gauge symmetry, the anomalon fields, and the spontaneous breaking of $U(1)_B$ symmetry by the complex scalar field Φ . In particular, we discuss the production and decay modes for the radial scalar mode of Φ . In Section 3, we reanalyze the phenomenology

when ϕ mixes with the SM Higgs boson, taking into account the current constraints from measurements of the 125 GeV Higgs boson. We conclude in Section 4.

2 Quark-universal $U(1)_B$ gauge symmetry

A quark-universal $U(1)_B$ gauge symmetry is a chiral gauge extension of the Standard Model gauge sector, since the global baryon number symmetry of the SM is anomalous with respect to $SU(2)_L$ and $U(1)_Y$. Hence, renormalizability of the theory requires adding new fermions (“anomalons”) to cancel the mixed $SU(2)_L^2 \times U(1)_B$ and $U(1)_Y^2 \times U(1)_B$ anomalies, and also must ensure no new gauge anomalies are introduced [23]. Furthermore, we introduce a scalar field Φ that acquires a vacuum expectation value (vev) to spontaneously break the $U(1)_B$ symmetry and generate masses for the Z' boson and anomalons, which is also a minimal construction consistent with renormalizability and perturbative unitarity [24, 25]. Hence, a renormalizable theory for a $U(1)_B$ gauge symmetry with quark-universal couplings is the fermion set [8, 10, 11]

$$\begin{aligned} L_L &\sim (2, -1/2, -1), & E_L &\sim (1, -1, 2), & N_L &\sim (1, 0, 2), \\ L_R &\sim (2, -1/2, 2), & E_R &\sim (1, -1, -1), & N_R &\sim (1, 0, -1), \end{aligned} \quad (2.1)$$

where representations under $SU(2)_L \times U(1)_Y \times U(1)_B$ are given, and we also introduce a complex scalar Φ that is a SM gauge singlet and carries $U(1)_B$ charge $z_\Phi = +3$. The N_L and N_R fields are necessary to cancel the $U(1)_B$ -gravitational anomaly and $U(1)_B^3$ anomalies [9, 10, 13, 14]. An additional feature of the above matter content is that the kinetic mixing between the SM Z boson and the Z' boson is only generated at 1-loop and is logarithmic below the mass scale of the anomalons [14]. A tree-level kinetic mixing can be forbidden given the theory is embedded in a non-Abelian ultraviolet completion and remains vanishing until the scale of the anamolons masses since the fermion content of the model satisfies the trace condition [14]. An important distinction from other studies of gauged baryon number [7, 16, 26] is that our anamolons sector is uncharged under $SU(3)_c$ symmetry, which dramatically alters the collider phenomenology for anamolons production as well as the radial mode of Φ .

Having established the matter content for the chiral $U(1)_B$ gauge symmetry, we now discuss the Lagrangian interactions, beginning with the scalar field Φ .

2.1 Scalar responsible for $U(1)_B$ breaking and anomalon masses

A renormalizable realization of the $U(1)_B$ spontaneous symmetry breaking is the Lagrangian,

$$\mathcal{L} = -\frac{1}{4}Z'_{\mu\nu}Z'^{\mu\nu} + |D_\mu\Phi|^2 - \mu_\Phi^2|\Phi|^2 - \lambda_\Phi|\Phi|^4, \quad (2.2)$$

where the covariant derivative is

$$D_\mu = \partial_\mu - 3i\frac{g_B}{2}Z'_\mu, \quad (2.3)$$

and $\mu_\Phi^2 < 0$ triggers spontaneous breaking of $U(1)_B$ via the vev $v' = \sqrt{|\mu_\Phi^2|/\lambda_\Phi}$, leaving the radial mode $\Phi = (v' + \phi)/\sqrt{2}$ (in unitary gauge). The $U(1)_B$ interactions for SM quarks are

$$\mathcal{L}_q = \frac{g_B}{6}Z'_\mu \sum_q \bar{q}\gamma^\mu q, \quad (2.4)$$

where q represents the six SM quark flavors, and the normalization accounts for the baryon charge (+1/3) of the SM quarks.

Discovering the physical real scalar ϕ at colliders is a necessary requirement to establish the spontaneous symmetry breaking nature of the Z' boson. Moreover, the ϕ scalar cannot be too heavy compared to the Z' boson, since the ϕ boson unitarizes longitudinal Z' scattering [25, 28]. The Z' mass is $M_{Z'} = 3\frac{g_B}{2}v'$.

The anomalons have the Yukawa Lagrangian

$$\begin{aligned} \mathcal{L}_{\text{Yuk}} = & -y_L\bar{L}_L\Phi^*L_R - y_E\bar{E}_L\Phi E_R - y_N\bar{N}_L\Phi N_R \\ & -y_1\bar{L}_L H E_R - y_2\bar{L}_R H E_L - y_3\bar{L}_L\tilde{H}N_R - y_4\bar{L}_R\tilde{H}N_L + \text{h.c.}, \end{aligned} \quad (2.5)$$

where H is the complex scalar Higgs doublet of the SM. The first line of Eq. (2.5) reflects the chiral nature of the anomalons under the $U(1)_B$ symmetry and the second line reflects the chiral nature under the SM gauge symmetries. We can use global $U(1)$ phase transformations on the fields to ensure that all the Yukawa couplings in (2.5) are real.

Note that Yukawa couplings of anomalons to SM leptons are forbidden by the $U(1)_B$ gauge symmetry. Even after $U(1)_B$ breaking, a remnant \mathbb{Z}_3 symmetry (a consequence of the $U(1)_B$ charge of Φ , $z_\Phi = 3$) still forbids such couplings. In extended models (not analyzed here) that include scalars with vevs that carry $U(1)_B$ charge 1 or 2, Yukawa couplings of anomalons to SM leptons would be allowed (see [27] for a study of their possible effects).

Since both Φ and H acquire vevs (v' and $v_h \approx 246$ GeV, respectively), the anomalon mass eigenstates are admixtures of the Weyl fermions in Eq. (2.1), with two Dirac fermions E_1 and E_2 of electric charge -1 and two Dirac fermions N_1 and N_2 that are electrically neutral. The E_1 and E_2 masses are

$$M_{1,2}^2 = \frac{1}{4} \left(v_h^2 (y_1^2 + y_2^2) + v'^2 (y_L^2 + y_E^2) \right) \left(1 \mp \sqrt{1 - \frac{4(v_h^2 y_1 y_2 - v'^2 y_L y_E)^2}{(v_h^2 (y_1^2 + y_2^2) + v'^2 (y_L^2 + y_E^2))^2}} \right). \quad (2.6)$$

The interaction and mass eigenstates for the charged anomalons are related by separate rotations for the left- and right-handed fields:

$$\begin{aligned} \begin{pmatrix} L_L^- \\ E_L \end{pmatrix} &= \begin{pmatrix} \cos \theta & \sin \theta \\ -\sin \theta & \cos \theta \end{pmatrix} \begin{pmatrix} E_{2L} \\ E_{1L} \end{pmatrix}, \\ \begin{pmatrix} L_R^- \\ E_R \end{pmatrix} &= \begin{pmatrix} \cos \chi & \sin \chi \\ -\sin \chi & \cos \chi \end{pmatrix} \begin{pmatrix} E_{2R} \\ E_{1R} \end{pmatrix}, \end{aligned} \quad (2.7)$$

where the θ and χ angles satisfy

$$\begin{aligned} \tan 2\theta &= \frac{2 v_h v' (y_L y_2 + y_E y_1)}{v'^2 (y_L^2 - y_E^2) + v_h^2 (y_1^2 - y_2^2)}, \\ \tan 2\chi &= \frac{2 v_h v' (y_L y_1 + y_E y_2)}{v'^2 (y_L^2 - y_E^2) - v_h^2 (y_1^2 - y_2^2)}. \end{aligned} \quad (2.8)$$

Interestingly, the Yukawa couplings in (2.5) can be analytically expressed in terms of the masses and mixing angles. To derive those relations for the charged anomalons, replace the scalars by their vevs in (2.5), then transform the fermions from the gauge eigenstates to mass basis. The 2×2 mass matrix obtained this way, with entries proportional to linear combinations of y_1, y_2, y_L, y_E , is then identified with the diagonal mass matrix for E_1 and E_2 . The ensuing four equations can be solved, with the result

$$\begin{aligned} y_L \pm y_E &= -\sqrt{2} \frac{(M_2 \pm M_1)}{v'} \cos(\theta \mp \chi), \\ y_2 \pm y_1 &= -\sqrt{2} \frac{(M_2 \mp M_1)}{v_h} \sin(\theta \pm \chi). \end{aligned} \quad (2.9)$$

Having both vectorlike and chiral mass generation for the anomalons implies the presence of off-diagonal Yukawa couplings as well as off-diagonal Z and Z' couplings in the

anomalon mass basis. We note that the photon couplings remain diagonal, as a consequence of the unbroken $U(1)_{\text{em}}$ symmetry. In the mass basis, the charged anomalons have Yukawa interactions with the ϕ scalar and the SM Higgs boson h_{SM}^0 , given by

$$\begin{aligned} \mathcal{L}_{\text{Yuk}} = & -\phi \bar{E}_1 \left(y_{11}^\phi E_1 + y_{12}^\phi E_2 \right) - \phi \bar{E}_2 \left(y_{21}^\phi E_1 + y_{22}^\phi E_2 \right) \\ & - h_{\text{SM}}^0 \bar{E}_1 \left(y_{11}^{h_{\text{SM}}} E_1 + y_{12}^{h_{\text{SM}}} E_2 \right) - h_{\text{SM}}^0 \bar{E}_2 \left(y_{21}^{h_{\text{SM}}} E_1 + y_{22}^{h_{\text{SM}}} E_2 \right) . \end{aligned} \quad (2.10)$$

Using Eqs. (2.9), we can express the above Yukawa couplings (times γ^5 in the case of some off-diagonal terms) solely in terms of the mixing angles, masses, and vevs; the ones to ϕ are

$$\begin{aligned} \left\{ y_{11}^\phi, y_{22}^\phi \right\} &= \frac{1}{2v'} \left(\mp (M_1 - M_2) \cos^2(\theta + \chi) + (M_1 + M_2) \cos^2(\theta - \chi) \right) , \\ \left\{ y_{12}^\phi, y_{21}^\phi \right\} &= \frac{1}{4v'} \left(-(M_1 - M_2) \sin 2(\theta + \chi) \pm (M_1 + M_2) \sin 2(\theta - \chi) \gamma^5 \right) , \end{aligned} \quad (2.11)$$

while the ones to h_{SM}^0 are

$$\begin{aligned} \left\{ y_{11}^{h_{\text{SM}}}, y_{22}^{h_{\text{SM}}} \right\} &= \frac{1}{2v_h} \left(\mp (M_1 - M_2) \sin^2(\theta + \chi) + (M_1 + M_2) \sin^2(\theta - \chi) \right) , \\ \left\{ y_{12}^{h_{\text{SM}}}, y_{21}^{h_{\text{SM}}} \right\} &= \frac{-v'}{v_h} \left\{ y_{12}^\phi, y_{21}^\phi \right\} . \end{aligned} \quad (2.12)$$

For later convenience, we write each coupling in (2.11) and (2.12) as

$$y_{ab}^X = y_{ab}^{X(S)} + y_{ab}^{X(P)} \gamma^5 , \quad (2.13)$$

where X here stands for ϕ or h_{SM} , and the superscripts (S) or (P) denote the scalar or pseudoscalar coupling in the given Yukawa coupling. These Yukawa couplings play an important role in mediating the loop-induced decays $\phi \rightarrow \gamma\gamma$, $Z'\gamma$, and $Z\gamma$ as well as $\phi \rightarrow Z'Z$, ZZ , and W^+W^- . Furthermore, they lead to corrections to the SM Higgs decay rates $h_{\text{SM}}^0 \rightarrow \gamma\gamma$ and $Z\gamma$, and induce the nonstandard modes $h_{\text{SM}}^0 \rightarrow Z'\gamma$ and $h_{\text{SM}}^0 \rightarrow Z'Z'$.

We remark that the off-diagonal couplings y_{12}^ϕ and y_{21}^ϕ vanish in the limit $y_1, y_2 \rightarrow 0$ for finite y_L and y_E , while an equivalent set of couplings $y_{11}^{h_{\text{SM}}}$ and $y_{22}^{h_{\text{SM}}}$ vanish in the limit $y_L, y_E \rightarrow 0$ for finite y_1, y_2 . Since y_1 and y_2 are constrained directly by the measured 125 GeV Higgs diphoton decay rate [19–21], we will focus on the regime $y_1, y_2 \ll y_L, y_E$ for $v' \sim v_h$, such that the dominant terms for the anomalon masses arise from the $U(1)_B$ breaking vev. Note that the Yukawa couplings in Eqs. (2.11) and (2.12) correspond to scalar states that are not mixed, and are readily amended to incorporate a scalar mixing angle between ϕ and h_{SM}^0 , as discussed in Sec. 3.

The Lagrangian for Z' and Z interactions with the charged anomalous in the mass eigenstate basis is

$$\begin{aligned} \mathcal{L}_{Z',Z} = & Z'_\mu \bar{E}_1 \gamma^\mu \left(g_{11}^{Z'} E_1 + g_{12}^{Z'} E_2 \right) + Z'_\mu \bar{E}_2 \gamma^\mu \left(g_{21}^{Z'} E_1 + g_{22}^{Z'} E_2 \right) \\ & + Z_\mu \bar{E}_1 \gamma^\mu \left(g_{11}^Z E_1 + g_{12}^Z E_2 \right) + Z_\mu \bar{E}_2 \gamma^\mu \left(g_{21}^Z E_1 + g_{22}^Z E_2 \right) , \end{aligned} \quad (2.14)$$

where the vector and axial-vector couplings are encoded by the following coefficients (times γ^5 in the case of some off-diagonal terms):

$$\begin{aligned} g_{11}^{Z'} &= \frac{g_B}{4} \left[(1 + 3 \sin^2 \theta - 3 \sin^2 \chi) + 3 (1 - \sin^2 \theta - \sin^2 \chi) \gamma^5 \right] , \\ g_{12}^{Z'} &= g_{21}^{Z'} = \frac{3}{8} g_B \left[\sin 2\theta - \sin 2\chi - (\sin 2\theta + \sin 2\chi) \gamma^5 \right] , \\ g_{22}^{Z'} &= \frac{g_B}{4} \left[(1 - 3 \sin^2 \theta + 3 \sin^2 \chi) - 3 (1 - \sin^2 \theta - \sin^2 \chi) \gamma^5 \right] \end{aligned} \quad (2.15)$$

for the Z' boson, and

$$\begin{aligned} g_{11}^Z &= \frac{g}{4c_W} \left[(4s_W^2 - \cos^2 \theta - \cos^2 \chi) - (\sin^2 \theta - \sin^2 \chi) \gamma^5 \right] , \\ g_{12}^Z &= g_{21}^Z = \frac{g}{8c_W} \left[\sin 2\theta + \sin 2\chi + (-\sin 2\theta + \sin 2\chi) \gamma^5 \right] , \\ g_{22}^Z &= \frac{g}{4c_W} \left[(4s_W^2 - \sin^2 \theta - \sin^2 \chi) + (\sin^2 \theta - \sin^2 \chi) \gamma^5 \right] \end{aligned} \quad (2.16)$$

for the Z boson. Again, for later convenience, the above Z' and Z couplings are written in terms of vector and axial-vector couplings, denoted by

$$g_{ab}^X = g_{ab}^{X(V)} + g_{ab}^{X(A)} \gamma^5 , \quad (2.17)$$

where X here stands for Z' or Z . It is straightforward to check that these couplings reduce to the expected diagonal couplings in the limit $\theta, \chi \rightarrow 0$.

For completeness, we also briefly list the W interactions with the charged and neutral anomalous, in the limit of vanishing neutral anomalon mixing when y_3 and y_4 are zero. The charged current Lagrangian is

$$\mathcal{L}_W = W_\mu^+ \bar{N}_2 \gamma^\mu \left(g_2^W E_2 + g_1^W E_1 \right) + \text{h.c.} . \quad (2.18)$$

The corresponding anomalon couplings to the W boson are

$$\begin{aligned} g_1^W &= \frac{g}{2\sqrt{2}} \left[-(\sin \theta + \sin \chi) + (\sin \theta - \sin \chi) \gamma^5 \right] , \\ g_2^W &= \frac{g}{2\sqrt{2}} \left[(\cos \theta + \cos \chi) - (\cos \theta - \cos \chi) \gamma^5 \right] . \end{aligned} \quad (2.19)$$

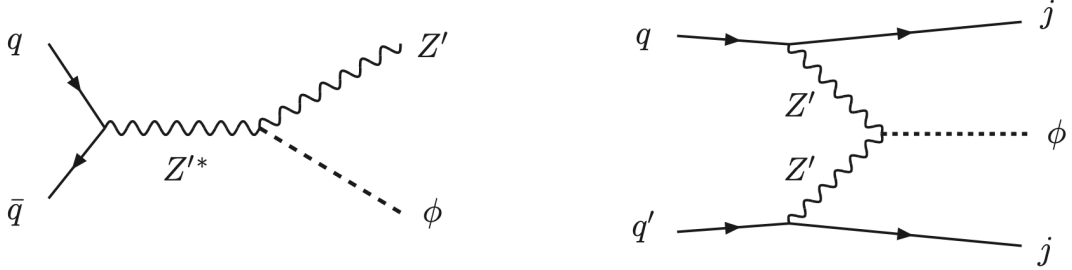


Figure 1: Production processes of the ϕ scalar at hadron colliders: associated $\phi Z'$ production through an off-shell Z' boson (left diagram), and Z' -fusion (right diagram).

2.2 Scalar production at hadron colliders

As the scalar associated with spontaneous breaking of a gauge symmetry, ϕ can be produced at the LHC via the intrinsic and diagnostic processes of ϕ -strahlung from Z' as well as Z' fusion, with Feynman diagrams shown in Figure 1. Another set of scalar production modes arise from anomalon pair production from electroweak interactions followed by decays involving ϕ , or by radiation of a ϕ ; as their cross sections are highly dependent on anomalon masses, we will ignore such processes in what follows.

We show the cross sections for $pp \rightarrow Z' \phi$ and $pp \rightarrow \phi jj$ via Z' -fusion in Figure 2 for $g_B = 0.3$ and two choices of the mass ratio, $M_{Z'}/M_\phi = 0.7$ or 1.3. Notably, with $g_B = 0.3$ at the 13.6 TeV LHC, the $Z' \phi$ cross section ranges from 1 fb to 1000 fb for M_ϕ ranging from 500 GeV to 50 GeV, while the Z' -fusion rate is roughly one or two orders of magnitude smaller. Given that $M_{Z'}$ is held fixed, the cross section for $Z' \phi$ production scales as g_B^4 , while the Z' -fusion rate scales as g_B^6 .

These rates were calculated using MadGraph_aMC@NLO [29] with model files generated by the FeynRules package [30]. The computation incorporates next-to-leading order (NLO) QCD corrections via FeynArts [31], and uses the default PDF set employed in Madgraph, NNPDF23_nlo_as_0119_qed [32].

We remark that these production processes are intrinsic to the spontaneous breaking by Φ of any new $U(1)$ gauge symmetry, and thus apply qualitatively to many Z' models. The $\phi - Z' - Z'$ vertex evident in both processes is emblematic of the Higgs mechanism. Furthermore, both cross sections are independent of the anomalon masses or charges. Nevertheless, the rates obtained for $U(1)_B$ cannot be directly used to compute the rates for different Z' couplings to the up and down quarks (initial states with heavier quarks have negligible contributions). The reason is that the ratio of the u and d PDFs depends

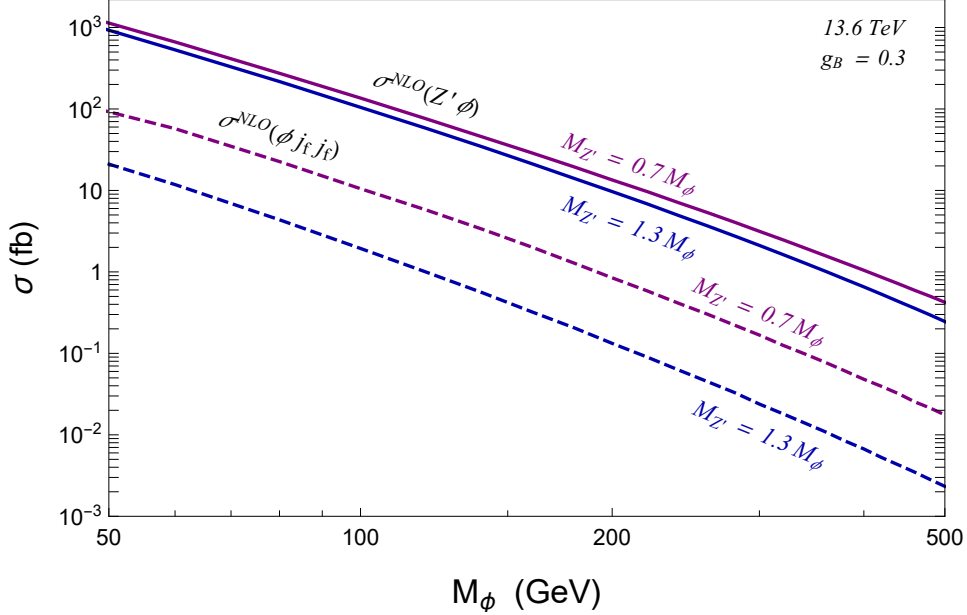


Figure 2: Cross sections at the 13.6 TeV LHC for ϕ production in association with a Z' (solid lines), and through Z' fusion (dashed lines, labelled $\phi j_f j_f$, where j_f is a forward jet), as a function of the ϕ mass. The $Z'\phi$ and $\phi j_f j_f$ cross sections are computed at NLO in α_s for $M_{Z'}/M_\phi = 0.7$ (upper lines) and 1.3 (lower lines), for a Z' gauge coupling $g_B = 0.3$; for fixed $M_{Z'}/M_\phi$, the cross section scales as g_B^4 for $Z'\phi$ production, and as g_B^6 for Z' fusion.

on the energy scale of the process, which in turn depends on $M_{Z'}$ and M_ϕ .

We now study the corresponding chiral symmetry breaking phenomenology for ϕ decays, assuming negligible mixing between the ϕ scalar and the SM Higgs boson. The situation when ϕ and h_{SM}^0 have sizable mixing is analyzed in Section 3.

2.3 Branching fractions of the scalar ϕ

The ϕ scalar, as the radial mode of the scalar field that spontaneously breaks a chiral gauge symmetry, exhibits a few classes of possible decays.

First, the ϕ scalar is expected to dominantly decay to a pair of Z' bosons, with one of them or even both being off-shell for $M_\phi < 2M_{Z'}$. The subsequent tree-level decays of $Z' \rightarrow jj$ give difficult but interesting 4-jet final states, where the 4-jet invariant mass peaks at M_ϕ , and include one or two dijet resonances peaked at $M_{Z'}$ when the corresponding Z'

is on-shell. The partial width for ϕ decaying into a pair of Z' bosons is given by (see [33])

$$\Gamma(\phi \rightarrow Z'Z'^{(*)}) = \begin{cases} \frac{9g_B^2}{128\pi} M_\phi R_2(M_{Z'}^2/M_\phi^2) & , \text{ for } M_\phi > 2M_{Z'} \\ \frac{5g_B^4}{1024\pi^3} M_\phi R_T(M_{Z'}^2/M_\phi^2) & , \text{ for } 2M_{Z'} > M_\phi > M_{Z'} \end{cases} , \quad (2.20)$$

where the second line is the 3-body decay $\phi \rightarrow Z'Z'^* \rightarrow Z'q\bar{q}$ summed over 5 SM quark flavors; following Ref. [33], we defined the functions

$$R_2(x) = \left(12x - 4 + \frac{1}{x}\right) \sqrt{1 - 4x} , \quad (2.21)$$

$$R_T(x) = 3 \frac{1 - 8x + 20x^2}{\sqrt{4x - 1}} \arccos\left(\frac{3x - 1}{2x^{3/2}}\right) - \frac{1 - x}{2x} (2 - 13x + 47x^2) - \frac{3}{2} (1 - 6x + 4x^2) \ln x . \quad (2.22)$$

As a second possibility, the ϕ scalar could in principle decay to pairs of anomalous via the Yukawa couplings in Eq. (2.10), but here we assume the anomalous are heavier than $M_\phi/2$, and thus this decay channel is kinematically closed. Another decay process is $\phi \rightarrow b\bar{b}$, which occurs at one loop, with two Z' bosons running in the loop together with a b quark. The partial width of this decay mode is suppressed not only by the loop factor, but also by $(m_b/M_{Z'})^2$. A similar $\phi \rightarrow t\bar{t}$ mode would occur through a less suppressed loop, but it is kinematically closed for the range of ϕ masses considered here.

More relevant are loop-induced decays of ϕ to pairs of gauge bosons through loops of anomalous. In particular, the anomalous give non-decoupling contributions to loop-induced decays $\phi \rightarrow \gamma\gamma, Z'\gamma, Z\gamma, Z'Z, ZZ$ and W^+W^- , where the last five modes can have additional phase-space suppression factors. Here, the nondecoupling of anomalous precisely follows the Higgs low-energy theorem from SM Higgs phenomenology [17, 18]. We also remark that the $\phi \rightarrow Z'Z$ diagram explicitly reintroduces Z' - Z mixing at the anomalon mass scale. Separately, for finite θ and χ , the anomalous introduce $\phi - h_{\text{SM}}^0$ mixing at one loop. Nonetheless, vanishing $\phi - h_{\text{SM}}^0$ mixing at one-loop can still be ensured by an appropriate choice of the Higgs portal coupling, hence we neglect these mixing diagrams and the anomalon contributions to the W and Z masses in this section. We explicitly study the effect of finite $\phi - h_{\text{SM}}^0$ mixing in the next section.

The 1-loop decay of ϕ into photons gets contributions from the E_1 and E_2 charged anomalous, giving

$$\Gamma(\phi \rightarrow \gamma\gamma) = \frac{\alpha^2 M_\phi^3}{256\pi^3} \left| \sum_{a=1}^2 \frac{y_{aa}^{\phi(S)}}{M_a} F_1\left(\frac{M_\phi^2}{4M_a^2}\right) \right|^2 , \quad (2.23)$$

where $y_{aa}^{\phi(S)}$ are given in Eqs. (2.13) and (2.11). The above loop function is [33]

$$F_1(x) = \frac{2}{x^2} \left[x + (x-1)Z(x) \right] , \quad (2.24)$$

with

$$Z(x) = \begin{cases} \frac{-1}{4} \left[2 \ln(\sqrt{x} + \sqrt{x-1}) - i\pi \right]^2 & , \text{ for } x > 1 \\ \arcsin^2(\sqrt{x}) & , \text{ for } x \leq 1 \end{cases} . \quad (2.25)$$

There are also intrinsic 1-loop decays into $Z'\gamma$ and $Z\gamma$, with decay widths given by

$$\Gamma(\phi \rightarrow X\gamma) = \frac{\alpha M_\phi^3 (1 - M_X^2/M_\phi^2)^3}{32\pi^4} \left| \sum_{a,b=1}^2 \frac{c_{ab}^{(X)}}{M_a} F^{X\gamma}(M_\phi, M_X, M_a, M_b) \right|^2 , \quad (2.26)$$

where $X = \{Z', Z\}$, and the coefficients $c_{ab}^{(X)}$ are defined as

$$c_{ab}^{(X)} = y_{ab}^{\phi(S)} g_{ab}^{X(V)} - y_{ab}^{\phi(P)} g_{ab}^{X(A)} . \quad (2.27)$$

Here y_{ab}^ϕ and g_{ab}^X are the Yukawa and gauge couplings given in Eqs. (2.13), (2.17), respectively, and the loop function is

$$\begin{aligned} F^{X\gamma}(M_\phi, M_X, M_a, M_b) = & \frac{2M_a^2}{M_\phi^2 - M_X^2} \left[\frac{B(M_\phi^2, M_a, M_b) - B(M_X^2, M_a, M_b)}{1 - M_\phi^2/M_X^2} - \frac{M_a^2 - M_b^2}{M_\phi^2} \ln\left(\frac{M_a}{M_b}\right) \right. \\ & \left. + \left(\frac{M_\phi^2 - M_X^2}{2} - M_a^2 \right) C_0(0, M_\phi^2, M_X^2, M_a, M_a, M_b) - M_b^2 C_0(0, M_\phi^2, M_X^2, M_b, M_b, M_a) - 1 \right] \end{aligned} \quad (2.28)$$

with B, C_0 being Passarino-Veltman loop functions [34] following the Package-X convention [35]. For $M_a = M_b$, $F^{X\gamma}(M_\phi, M_X, M_a, M_a) = F_2\left(\frac{4M_a^2}{M_\phi^2}, \frac{4M_a^2}{M_X^2}\right)$, where the F_2 loop function is adapted from [33]:

$$F_2(x, y) = \frac{xy}{2(x-y)} \left[1 + \left(1 + \frac{xy}{x-y} \right) \left(Z(x^{-1}) - Z(y^{-1}) \right) + 2x \frac{g(x^{-1}) - g(y^{-1})}{x-y} \right] , \quad (2.29)$$

with

$$g(x) = \begin{cases} \sqrt{1/x-1} \arcsin(\sqrt{x}) & , \text{ for } x \leq 1 \\ \sqrt{1-1/x} \left[\ln(\sqrt{x} + \sqrt{x-1}) - i\pi/2 \right] & , \text{ for } x > 1 \end{cases} . \quad (2.30)$$

Lastly, ϕ also decays into pairs of massive gauge bosons at one-loop. Since the charged anomalons have both $U(1)_B$ and EW vev contributions to their masses, their couplings to ϕ , Z , and Z' are generally flavor-violating, as shown in Sec. 2.1. Hence, we present the corresponding decay width calculations for $\phi \rightarrow Z'Z$, ZZ , and W^+W^- with the reference matrix elements shown in Fig. 3a for ϕ decaying to two on-shell massive vectors and Fig. 3b for ϕ decaying to a three-body final state of SM particles.

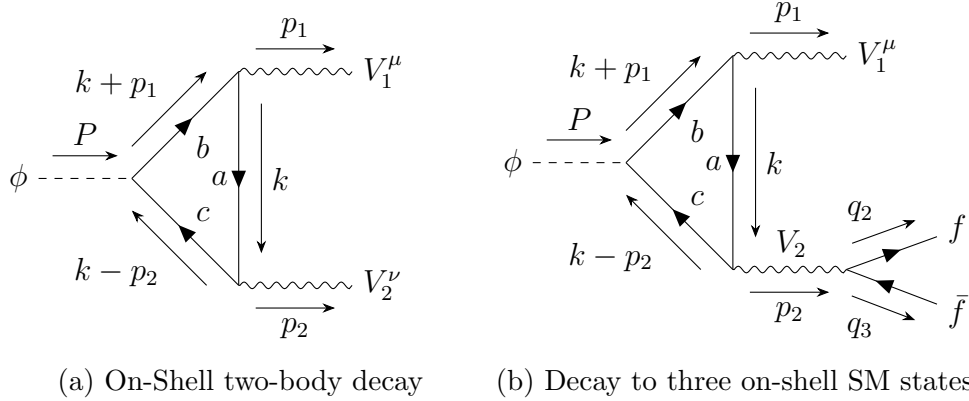


Figure 3: Feynman diagrams for ϕ decay to (a) generic vector boson final states V_1 , V_2 and (b) $V_1 f \bar{f}$, where the intermediate fermions labeled a , b , and c denote all possible combinations of anomalons. The diagrams with reversed fermion flow are implicitly included.

The matrix elements for Fig. 3 are then

$$\begin{aligned}
 i\mathcal{M}_{abc}(\phi \rightarrow V_1 V_2) &= -\epsilon_\mu^*(p_1)\epsilon_\nu^*(p_2) \int \frac{d^4 k}{(2\pi)^4} \\
 &\quad \text{Tr} \left[\frac{\not{k} + M_a}{k^2 + M_a^2} \gamma^\mu (ig_{ab}^{V_1}) \frac{\not{k} + \not{p}_1 + M_b}{(k + p_1)^2 - M_b^2} (-iy_{bc}^\phi) \frac{\not{k} - \not{p}_2 + M_c}{(k - p_2)^2 - M_c^2} \gamma^\nu (ig_{ca}^{V_2}) \right]
 \end{aligned} \tag{2.31}$$

and

$$\begin{aligned}
 i\mathcal{M}_{abc}(\phi \rightarrow V_1 f \bar{f}) &= -\epsilon_\mu^*(p_1) \left(\frac{-ig_{\nu\alpha}}{(q_2 + q_3)^2 - M_{V_2}^2} \bar{u}(q_2) \gamma^\alpha (ig_{f\bar{f}}^{V_2}) v(q_3) \right) \int \frac{d^4 k}{(2\pi)^4} \\
 &\quad \text{Tr} \left[\frac{\not{k} + M_a}{k^2 + M_a^2} \gamma^\mu (ig_{ab}^{V_1}) \frac{\not{k} + \not{p}_1 + M_b}{(k + p_1)^2 - M_b^2} (-iy_{bc}^\phi) \frac{\not{k} - \not{p}_2 + M_c}{(k - p_2)^2 - M_c^2} \gamma^\nu (ig_{ca}^{V_2}) \right],
 \end{aligned} \tag{2.32}$$

where V_1 and V_2 refer to $Z'Z$, ZZ , and W^+W^- , respectively. For the three-body decay, we assume that the final state SM fermions are massless, and the partial width coherently sums over all accessible SM fermions with their respective gauge couplings to W or Z . The

total matrix elements are readily computed from the above generic matrix elements, taking into account the diagrams with reversed fermion flow and the flavor-conserving and flavor-violating couplings shown in Sec. 2. For completeness, we also show the corresponding phase space integrations for the two-body $\phi \rightarrow V_1 V_2$ partial decay,

$$\Gamma(\phi \rightarrow V_1 V_2) = \frac{1}{16\pi M_\phi^3} \sqrt{\lambda(M_\phi^2, M_{V_1}^2, M_{V_2}^2)} |\mathcal{M}(\phi \rightarrow V_1 V_2)|^2 \quad (2.33)$$

with λ denoting the Källén- λ function, and the $\phi \rightarrow V f \bar{f}$ partial decay,

$$\Gamma(\phi \rightarrow V_1 f \bar{f}) = \frac{1}{(2\pi)^3} \frac{1}{32M_\phi^3} \int_{M_{V_1}^2}^{M_\phi^2} dM_{12}^2 \int_0^{4E_f E_{\bar{f}}} dM_{23}^2 |\mathcal{M}(\phi \rightarrow V_1 f \bar{f})|^2 \quad (2.34)$$

where we used

$$E_f E_{\bar{f}} \approx \frac{1}{4M_{12}^2} (M_{12}^2 - M_{V_1}^2) (M_\phi^2 - M_{12}^2) , \quad (2.35)$$

and $M_{12}^2 = (p_1 + q_2)^2$ and $M_{23}^2 = (q_2 + q_3)^2$. All of these expressions are the dominant decay widths necessary to understand the collider phenomenology of ϕ decay modes when $\phi - h_{\text{SM}}^0$ mixing is absent but where anomalon mixing angles θ and χ are present.

The branching fractions of ϕ are shown in Figure 4 as a function of ϕ mass and two choices of $M_{Z'} = 70$ GeV or 100 GeV. For both choices of $M_{Z'}$, we set one charged anomalon mass to 200 GeV and the other to 250 GeV, with anomalon mixing angles of $\theta = 0.3$ and $\chi = 0.25$, adjusting the Yukawa couplings accordingly. We remark that the resulting Yukawa couplings are hierarchical with $y_1, y_2 \ll y_L, y_E$ and thus the modification of $B(h \rightarrow \gamma\gamma)$ is less than one percent [13]. In addition, the anomalons can be produced at the LHC via Drell-Yan processes, but their collider signatures into charged pions and missing transverse energy are difficult to detect [14].

For the ϕ mass range shown, the nominally leading decay, $\phi \rightarrow Z' Z'^{(*)}$, can be a 3-body process and becomes kinematically suppressed for lighter M_ϕ . Hence, the loop-induced decay $\phi \rightarrow \gamma\gamma$ becomes comparable to the $Z' Z'^{(*)}$ decay and in fact dominates for light ϕ masses. The other loop-induced decays to $Z'\gamma$, W^+W^- , and ZZ can also have percent-level branching fractions, and their complementary collider signatures are important to detect in order to extract the underlying pattern of anomalon masses and couplings. At a subleading rate, we can also expect the $Z\gamma$ decay. Importantly, the $\phi \rightarrow Z f \bar{f}$ partial width is mediated by one-loop amplitudes $\phi \rightarrow Z Z'^*$ and $\phi \rightarrow Z Z^*$ and their interference, which is included in Figure 4 (where the final state SM fermions are assumed massless). We have verified that the interference with the loop-induced coupling $\phi \rightarrow Z\gamma$, with γ

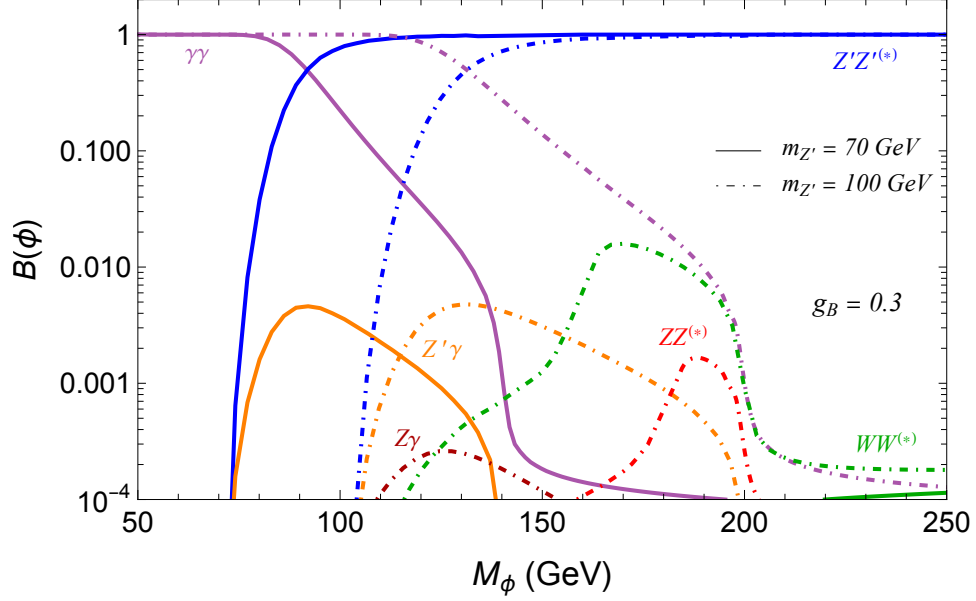


Figure 4: Branching fractions for the $U(1)_B$ -breaking scalar ϕ as a function of its mass. The parameters fixed here are $g_B = 0.3$, $M_{Z'} = 70$ GeV (solid lines) or $M_{Z'} = 100$ GeV (dashed lines), and negligible mixing with the SM Higgs boson. For the loop decays, $\phi \rightarrow \gamma\gamma$, $Z'\gamma$, $Z\gamma$, $ZZ^{(*)}$, and $WW^{(*)}$, we set the lighter anomalon mass to 200 GeV and the heavier to 250 GeV. The anomalon mixing angles are fixed to $\theta = 0.3$ and $\chi = 0.25$.

off-shell, is negligible. The branching fraction for $\phi \rightarrow Z'Z$ falls below 10^{-4} and is not shown. We remark that the branching ratio of $\phi \rightarrow WW^{(*)}$ and $\phi \rightarrow ZZ^{(*)}$ compared to $\phi \rightarrow Z'Z'^*$ reflects the mass hierarchy of the electroweak gauge boson masses compared to the Z' mass.

This pattern of decays from on-shell $Z'Z'$ for large ϕ masses to $\gamma\gamma$ for small ϕ masses is characteristic of scalars spontaneously breaking chiral gauge symmetries, and is reminiscent of SM Higgs phenomenology. In particular, for fixed gauge and chiral fermion masses, the heavy scalar limit necessarily corresponds to an enhanced coupling to longitudinal gauge bosons and the on-shell decay to two vector bosons saturates the decay width of the scalar. At the opposite end, the light scalar limit has a total decay width dominated by the nondecoupling loop effects of chiral fermions, which mediate decays to any and all kinematically allowed spectator bosons.

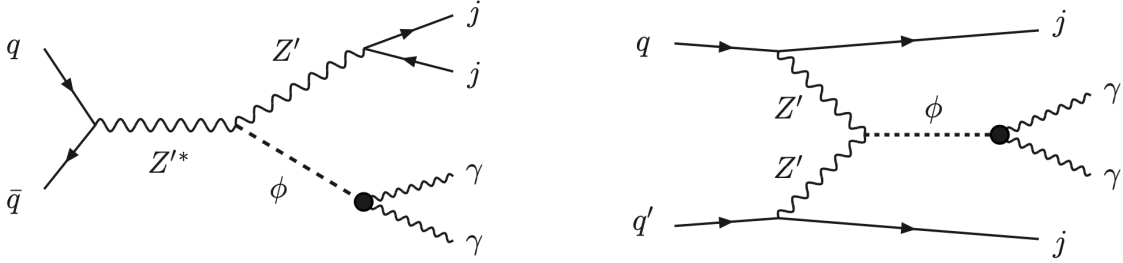


Figure 5: LHC signals of ϕ in the low- $M_\phi/M_{Z'}$ range, $M_\phi \lesssim 1.5M_{Z'}$: $(\gamma\gamma)(jj)$ (left diagram) and $(\gamma\gamma)j_f j_f$ (right diagram). The (jj) notation refers here to a dijet resonance at $M_{Z'}$, while j_f is a forward jet, as typically produced in Z' fusion.

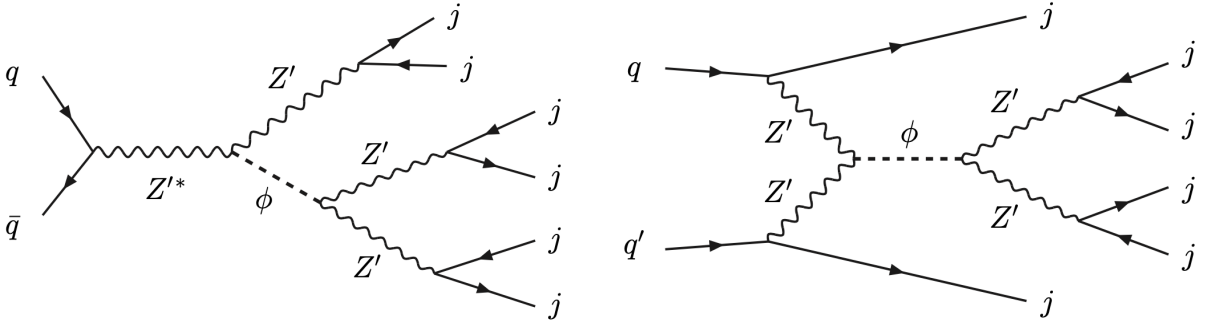


Figure 6: LHC signals of ϕ in the high- $M_\phi/M_{Z'}$ range, $M_\phi > 2M_{Z'}$: $3(jj)$ (left diagram) and $(jj)(jj)j_f j_f$ (right diagram).

2.4 LHC signals of the ϕ scalar

Having presented the LHC production modes and decay widths for ϕ , we now discuss the collider phenomenology of the ϕ scalar responsible for $U(1)_B$ breaking. Since the cross sections for ϕ production (see Figure 2) fall rapidly with increasing ϕ and Z' masses, we focus on mass ranges below a few hundred GeV. To analyze the LHC signals, we consider three intervals for the $M_\phi/M_{Z'}$ ratio.

2.4.1 Low $M_\phi/M_{Z'}$

For the “low- $M_\phi/M_{Z'}$ range”, $M_\phi \lesssim 1.5M_{Z'}$, the main decay mode of ϕ , with a branching fraction above 60%, is $\phi \rightarrow \gamma\gamma$. In this case associated ϕ production leads to a signal that involves a $\gamma\gamma$ resonance at M_ϕ plus a dijet resonance at $M_{Z'}$, as shown in the left panel of Figure 5. The ϕ production via Z' fusion also leads to a signal (see right panel of Figure 5) with a $\gamma\gamma$ resonance at M_ϕ , but the additional two jets do not form a resonance,

and are mostly in the forward region. We will refer to these two signals as $(\gamma\gamma)(jj)$ and $(\gamma\gamma)j_f j_f$, respectively, where (jj) denotes a dijet resonance at $M_{Z'}$, while j_f denotes a forward jet as typically produced in Z' fusion.

To illustrate the LHC capabilities in the low- $M_\phi/M_{Z'}$ range, we consider two points in the parameter space: $g_B = 0.3$, $M_\phi = 100$ GeV, and $M_{Z'} = 70$ GeV or $M_{Z'} = 130$ GeV. From Figures 2 and 4 follows that for $M_{Z'} = 70$ GeV the cross section at $\sqrt{s} = 13.6$ TeV times branching fraction for $\phi \rightarrow \gamma\gamma$ is $\sigma(pp \rightarrow Z'\phi)B(\phi \rightarrow \gamma\gamma) \approx 130$ fb. Thus, about 4×10^4 $(\gamma\gamma)(jj)$ events will be produced in Run 3 of the LHC, while the number of $(\gamma\gamma)j_f j_f$ will be smaller by a factor of approximately 10. The latter signal has only been studied by CMS and ATLAS in the context of the SM Higgs [36, 37], or when exotic final states such as dark photons are combined with forward jet tags [38]. Our analysis demonstrates that Z' -fusion provides a parametrically new analysis channel for nonstandard scalar production at the LHC.

Requiring two photons whose invariant mass distribution forms a peak reduces considerably the background, which is due to real photon emission but also due to QCD with jets misidentified as photons. The additional two jets, which either form a resonance at $M_{Z'}$ or are forward, may be used to further reduce the background.

2.4.2 High $M_\phi/M_{Z'}$

For the “high- $M_\phi/M_{Z'}$ range” $M_\phi > 2M_{Z'}$, the dominant decay mode is $\phi \rightarrow Z'Z'$, with a branching fraction above 99%. Associated ϕ production leads to a $3Z'$ signal, *i.e.*, six jets arranged in three dijet resonances, each of them at $M_{Z'}$, as shown in the left panel of Figure 6. We refer to this as the $3(jj)$ signal, where (jj) is a dijet resonance at $M_{Z'}$, but note that two of the dijets also form a 4-jet resonance at M_ϕ . Production of ϕ via Z' fusion gives a $Z'Z'j_f j_f$ signal, *i.e.*, six jets arranged in two dijet resonances at $M_{Z'}$ plus two forward jets, with the two dijets forming a 4-jet resonance at M_ϕ , as shown in the right panel of Figure 6. We refer to this as the $(jj)(jj)j_f j_f$ signal.

These signals suffer from large QCD backgrounds. These may be mitigated by requiring that one of the Z' decays into $b\bar{b}$. As the $Z' \rightarrow b\bar{b}$ branching fraction is 20%, the $(jj)(jj)(b\bar{b})$ signal (where j may or may not be a b jet) has a combined branching fraction of 49%, while $(jj)(b\bar{b})j_f j_f$ signal has a combined branching fraction of 36%. It is also possible to consider boosted topologies to reduce the background, again at the expense of a lower signal. In the case of associated ϕ production, if the $\phi \rightarrow (jj)(jj)$ system is boosted due to a high p_T of the $Z' \rightarrow (jj)$ system, then the final state would involve two

wide jets, one with 4-prong substructure, and one with a 2-prong substructure. Another possibility is to require an initial jet radiated with high p_T , so that either ϕ or Z' or both are boosted.

2.4.3 Intermediate $M_\phi/M_{Z'}$

In the intermediate- $M_\phi/M_{Z'}$ range $1.5 \lesssim M_\phi/M_{Z'} < 2$, the competition between the $\phi \rightarrow \gamma\gamma$ and $\phi \rightarrow Z'Z'_B \rightarrow Z'jj$ branching fractions makes it useful to search for both the lower-background signals involving a pair of photons and the $6j$ signals. The latter are labelled $(jj)(jj)jj$ and $(jj)(jj)j_fj_f$, while the former are labelled the same way as in the low-mass case. For the $6j$ signals, the background reduction methods discussed for the high-mass range also apply here, with the only difference that only two of the four narrow jets inside the ϕ wide jet form a resonance at $M_{Z'}$. On the other hand, the diphoton final state follows the same strategy as the low $M_\phi/M_{Z'}$ case. We remark that the 1-loop decays to ZZ and WW could potentially be seen in Higgs observables, although the expected rates imply that these effects would not serve as discovery channels.

To close this section, we remark that our focus on ϕ and Z' masses below a few hundred GeV precludes $Z' \rightarrow t\bar{t}$ decays. However, the case where $M_{Z'} \gtrsim 400$ GeV is also interesting (albeit the branching fraction for $Z' \rightarrow t\bar{t}$ remains below $1/6$). In particular, for $M_\phi < M_{Z'}$ that case leads to the $(\gamma\gamma)(t\bar{t})$ signature.

Having analyzed the situation where ϕ has negligible mixing with the SM Higgs boson, we now consider the collider phenomenology when mixing is included.

3 Effects of Higgs mixing

In this section, we consider the phenomenology of the new scalar in the presence of the Higgs portal coupling $|\Phi|^2 H^\dagger H$. The mass mixing between the ϕ scalar and the SM Higgs boson h_{SM}^0 leads to two mass eigenstates: the new physical scalar φ and h^0 , which is identified with the discovered Higgs boson with a mass near 125 GeV. Aside from mass mixing, the Higgs portal coupling leads to exotic decays such as $h^0 \rightarrow \varphi\varphi$ or $\varphi \rightarrow h^0 h^0$, depending on the scalar masses.

We begin with the full scalar potential,

$$V(\Phi, H) = \lambda_\Phi \left(|\Phi|^2 - \frac{v_0^2}{2} \right)^2 + \lambda_H \left(H^\dagger H - \frac{v_0^2}{2} \right)^2 + 2\lambda_p |\Phi|^2 H^\dagger H, \quad (3.1)$$

where the mass parameters v_0 and v'_0 are real and can be taken positive, the dimensionless quartic couplings satisfy $0 < \lambda_\Phi, \lambda_H \lesssim 1$, and the portal coupling λ_p is a real dimensionless parameter with $|\lambda_p| \ll 1$. Minimizing the potential gives the vacuum expectation values (vevs) $\langle \Phi \rangle = v'/\sqrt{2}$ and $\langle H \rangle = (0, v_h)^\top/\sqrt{2}$, with

$$\begin{aligned} v'^2 &= \lambda_H \frac{\lambda_\Phi v_0'^2 - \lambda_p v_0^2}{\lambda_H \lambda_\Phi - \lambda_p^2} , \\ v_h^2 &= \lambda_\Phi \frac{\lambda_H v_0^2 - \lambda_p v_0'^2}{\lambda_H \lambda_\Phi - \lambda_p^2} . \end{aligned} \quad (3.2)$$

Expanding $V(\Phi, H)$ around the vevs gives the scalar mass terms

$$-\frac{1}{2} \begin{pmatrix} \phi & h_{\text{SM}}^0 \end{pmatrix} \begin{pmatrix} 2\lambda_\Phi v'^2 & 2\lambda_p v_h v' \\ 2\lambda_p v_h v' & 2\lambda_H v_h^2 \end{pmatrix} \begin{pmatrix} \phi \\ h_{\text{SM}}^0 \end{pmatrix} , \quad (3.3)$$

leading to a scalar mixing angle α_h which satisfies

$$\tan(2\alpha_h) = \frac{2\lambda_p v_h v'}{\lambda_\Phi v'^2 - \lambda_H v_h^2} , \quad (3.4)$$

and defines the scalar mass eigenstates as

$$\begin{pmatrix} \varphi \\ h^0 \end{pmatrix} = \begin{pmatrix} \cos \alpha_h & \sin \alpha_h \\ -\sin \alpha_h & \cos \alpha_h \end{pmatrix} \begin{pmatrix} \phi \\ h_{\text{SM}}^0 \end{pmatrix} . \quad (3.5)$$

The properties of the physical particle h^0 are modified from the SM predictions by the above mixing. Given the good agreement of the SM predictions with the increasingly precise measurements of the Higgs production cross sections and branching fractions performed by the ATLAS and CMS collaborations, it must be that $|\sin \alpha_h|^2 \ll 1$. Thus, we can expand in α_h , which simplifies the relations between physical observables and the vevs. We obtain

$$\sin \alpha_h \approx \frac{\lambda_p v_h v'}{\lambda_\Phi v'^2 - \lambda_H v_h^2} , \quad (3.6)$$

and the scalar physical masses:

$$\begin{aligned} M_\varphi &\simeq \sqrt{\lambda_\Phi} v' \left(1 + \frac{2\lambda_p v_h}{\lambda_\Phi v'} \sin \alpha_h \right) , \\ M_h &\simeq \sqrt{\lambda_H} v_h \left(1 - \frac{2\lambda_p v'}{\lambda_H v_h} \sin \alpha_h \right) . \end{aligned} \quad (3.7)$$

Because the two scalar states are widely separated in mass, their effects on observables are factorized on their distinct pole masses. The complications arising when the mixing

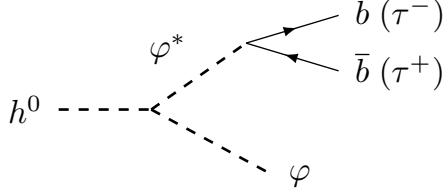


Figure 7: Three-body decay of the SM-like Higgs boson.

angle is large as well as when the states are nearly degenerate were recently addressed in [39].

In the remainder of this Section, we analyze the effects of the trilinear scalar interactions, and then the modifications of the Higgs boson properties.

3.1 Higgs decay $h^0 \rightarrow \varphi\varphi^{(*)}$ or resonant diHiggs process $\varphi \rightarrow h^0 h^0$

The extended Higgs Lagrangian not only mixes h_{SM}^0 and ϕ , it also introduces three-point vertices including combinations of h^0 and φ . For $M_h > M_\varphi$, this results at leading order in 3-body decays of the SM-like Higgs into φ and a pair of SM particles, whose width is highly dependent on the accessible phase space. For $M_h > 2M_\varphi$, both scalars are on-shell which increases the Higgs width by a tree-level decay into a φ pair. The $\varphi\varphi h^0$ and $\varphi h^0 h^0$ couplings in the Lagrangian can be written as

$$-\mu_{\varphi\varphi h} \varphi \varphi h^0 - \mu_{\varphi h h} \varphi h^0 h^0 \quad , \quad (3.8)$$

where the trilinear couplings have mass-dimension one. Keeping in mind that there may be large hierarchies between λ_p , λ_H , λ_Φ , and also that the ratio v_h/v' may be small, we expand in $\sin \alpha_h$ and find

$$\mu_{\varphi\varphi h} \simeq \lambda_p v_h - (3\lambda_\Phi - 2\lambda_p)v' \sin \alpha_h \quad . \quad (3.9)$$

For reference, the coupling

$$\mu_{\varphi h h} \simeq \lambda_p v' + (3\lambda - 2\lambda_p)v_h \sin \alpha_h \quad , \quad (3.10)$$

in the small angle approximation.

For the mass interval $M_h/2 < M_\varphi < M_h$, the SM-like Higgs boson can have 3-body decays

$$h^0 \rightarrow \varphi b\bar{b} \text{ or } \varphi \tau^+ \tau^- \quad . \quad (3.11)$$

Other tree-level 3-body decays are suppressed either by phase-space (*e.g.*, $h^0 \rightarrow \varphi W^{(*)}W^*$) or by smaller couplings (*e.g.*, $h^0 \rightarrow \varphi c\bar{c}$). The one-loop 3-body decay $h^0 \rightarrow \varphi gg$ is less interesting due to larger backgrounds; its contribution to the Higgs width is only about 10% of the contributions from (3.11), and we will ignore it in what follows.

The squared matrix element for the Feynman diagram shown in Figure 7 reads

$$|\mathcal{M}(h^0 \rightarrow \varphi b\bar{b})|^2 \approx \frac{2\mu_{\varphi\varphi h}^2 M_b^2 M_{23}^2 \sin^2\alpha_h}{v_h^2 (M_{23}^2 - M_\varphi^2)^2} , \quad (3.12)$$

where M_b is the b quark mass, corrections of order M_b/M_h are neglected, and M_{23} is the invariant mass of the fermion pair. The 3-body decay width is given by

$$\begin{aligned} \Gamma(h^0 \rightarrow \varphi b\bar{b}) &= \frac{1}{2^7 \pi^3 M_h^3} \int_{M_\varphi^2}^{M_h^2} dM_{12}^2 \int_0^{4E_b E_{\bar{b}}} dM_{23}^2 |\mathcal{M}(h^0 \rightarrow \varphi b\bar{b})|^2 \\ &= \frac{\mu_{\varphi\varphi h}^2 M_b^2 \sin^2\alpha_h}{64\pi^3 M_h v_h^2} R_S(M_\varphi^2/M_h^2) , \end{aligned} \quad (3.13)$$

with the function R_S defined by

$$R_S(x) = \frac{5x-1}{\sqrt{1-4x}} \operatorname{arccosh}\left(\frac{3x-1}{2x^{3/2}}\right) - (x-1) \left(\frac{1}{2} \ln x - 2\right) . \quad (3.14)$$

In deriving (3.13) we used a kinematic constraint on the product of b quark energies:

$$E_b E_{\bar{b}} \approx \frac{1}{4M_{12}^2} (M_{12}^2 - M_\varphi^2) (M_h^2 - M_{12}^2) . \quad (3.15)$$

An equivalent expression for $\Gamma(h^0 \rightarrow \varphi\tau^+\tau^-)$ can be obtained by substituting M_b^2 in (3.12) and (3.13) by $M_\tau^2/3$ to account for the τ mass and the sum over colors. For $M_\varphi < M_h/2$, both scalars get on-shell and the corresponding decay width is

$$\Gamma(h^0 \rightarrow \varphi\varphi) = \frac{\mu_{\varphi\varphi h}^2}{8\pi M_h} \left(1 - \frac{4M_\varphi^2}{M_h^2}\right)^{1/2} . \quad (3.16)$$

The constraint on the undetected Higgs width is $0.12 \times$ the SM Higgs width of $\Gamma_{\text{SM}}(h^0) \approx 4$ MeV [21], which excludes parts of the parameter space at small M_φ and different choices of $M_{Z'}$ and $\sin\alpha_h$, as shown in Figure 8. However, for $M_\varphi > M_h/2$, the $h^0 \rightarrow \varphi\varphi^*$ partial width is the only new contribution to the Higgs width, and it is negligible.

For $M_\varphi > M_h$, a decay of the SM-like Higgs into φ opens up, which for $M_\phi < 2M_h$ is a three body decay, and for $M_\phi > 2M_h$ is tree level. The decay width can be derived analogously to the first case by changing $c_{\varphi\varphi h} \rightarrow c_{\varphi h h}$ and $\sin\alpha_h \rightarrow \cos\alpha_h$. However, the decay of φ into $h^0 h^0$ is again negligible, since for very heavy M_ϕ the $Z'Z'$ decay dominates.

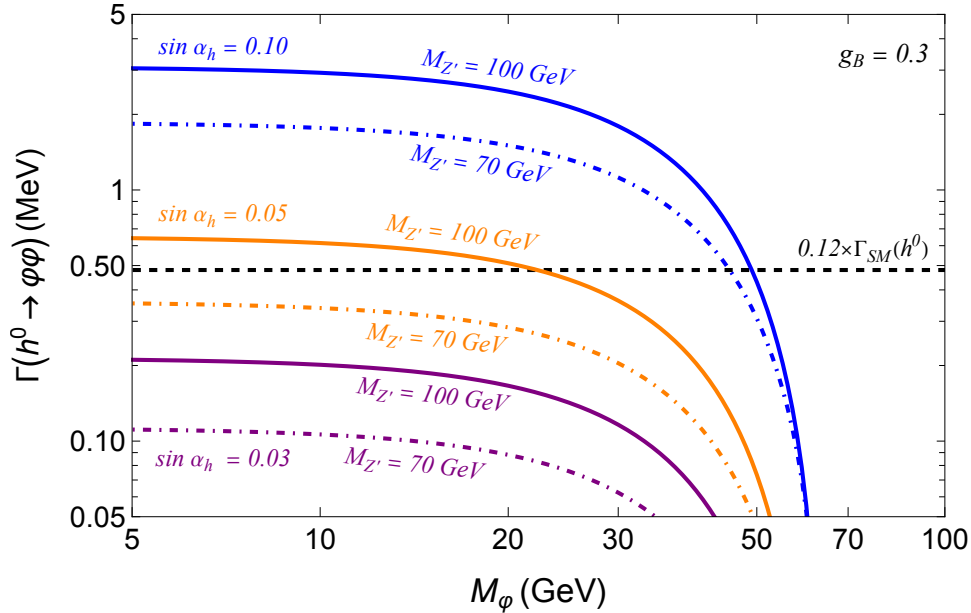


Figure 8: Decay width of the SM-like Higgs boson into $\varphi\varphi^{(*)}$, including the 3-body decay through an off-shell φ for $M_\varphi \lesssim M_h/2$. The parameters fixed here are $M_{Z'} = 70$ GeV (solid) or 100 GeV (dot-dashed), $g_B = 0.3$, and $\sin \alpha_h = 0.1, 0.05, 0.03$. The $0.12 \Gamma_{\text{SM}}(h^0)$ upper limit (dashed) with $\Gamma_{\text{SM}}(h^0) = 4$ MeV on undetected Higgs decays [21].

3.2 Mixing effects on the 125 GeV Higgs-like scalar h^0 and φ

If there is a sizable $\phi - h_{\text{SM}}^0$ mixing, then φ may also be produced by itself through gluon fusion; the cross section for this 1-loop process scales as $\sin^2 \alpha_h$ (assuming negligible 2-loop contributions induced by the $Z'Z'\varphi$ coupling), and is shown in Figure 9. Other mixing-suppressed production modes of φ , analogous with those of the SM Higgs, may also be relevant. In addition, φ may be pair produced in SM Higgs decays: $h \rightarrow \varphi\varphi$ for $M_\varphi < M_h/2$.

The constraints for the mixing angle can be calculated from the Higgs signal strengths $\mu_{\text{CMS}} = 1.002 \pm 0.057$ in [19] and $\mu_{\text{ATLAS}} = 1.05 \pm 0.06$ in [20]. These give a naive global average $\mu_{\text{LHC}} = 1.026 \pm 0.041$, implying

$$\sin \alpha_h \leq 0.24 \quad . \quad (3.17)$$

To satisfy this bound, we will adopt the choice of $\sin \alpha_h = 0.1, 0.05, \text{ or } 0.03$ in this work.

3.2.1 Production modes for φ

In Figure 9, we show the cross sections for ϕ production with $\sin\alpha_h = 0.05$, using MCFM [41, 42] for the cross sections based on rescaling SM Higgs rates. We can see, in comparison to the unmixed case in Figure 2, that the dominant production mode becomes gluon fusion, $gg \rightarrow \varphi$, for φ masses above 100 GeV and our specified $\sin\alpha_h = 0.05$, while Z' -associated production dominates for low φ masses. Given the scaling of Z' -associated production by g_B^4 and the scaling of gluon fusion by $\sin\alpha_h^2$, this crossover point between dominant production modes is highly model-dependent. We can see that the next most important production mode is the sum over Z' -fusion and SM vector boson fusion modes, which surpass the Z' -associated production modes for high φ masses, as already seen in Figure 2. We also show the important $\varphi + \geq 1(e, \mu, \tau)$ production rates, summing over the leptonic $W^\pm\varphi$ and $Z\varphi$ rates induced by $\sin\alpha_h$. Although these rates are roughly two orders of magnitude smaller than the Z' -associated modes, we believe optimized analyses for each the resonant dijet + φ signature from Z' -associated production and the lepton + φ signature can have competitive sensitivity, given the corresponding SM backgrounds, respectively. An analysis for the Z' -fusion mode can also reduce SM backgrounds by focusing on the two forward jet signature.

3.2.2 Decay modes of φ

When $\phi - h_{\text{SM}}^0$ mixing is nonzero, the interference between anomalon-induced processes and SM loop-induced processes is significant, primarily reflecting the underlying chiral symmetry respected by each sector of loop particles and fundamental spin statistics. We remark that even though ϕ is a gauge singlet, the non-trivial interference effects evident in the φ decay widths is a marked departure from the simplistic mixing-angle suppressed SM Higgs-like phenomenology that is commonly considered.

The new expression for the 1-loop decay of φ into photons gets contributions from the W and top quark, which are suppressed by the $\sin\alpha_h$ mixing, but also non-suppressed contributions from anomalon loops:

$$\Gamma(\varphi \rightarrow \gamma\gamma) = \frac{\alpha^2 M_\varphi^3}{256\pi^3} \left| \cos\alpha_h \sum_{a=1}^2 \frac{y_{aa}^{\phi(S)}}{M_a} F_1\left(\frac{M_\varphi^2}{4M_a^2}\right) + \sin\alpha_h \sum_{a=1}^2 \frac{y_{aa}^{h_{\text{SM}}(S)}}{M_a} F_1\left(\frac{M_\varphi^2}{4M_a^2}\right) + \frac{\sin\alpha_h}{v_h} \left[F_V\left(\frac{M_\varphi^2}{4M_W^2}\right) + \frac{4}{3} F_1\left(\frac{M_\varphi^2}{4M_t^2}\right) \right] \right|^2, \quad (3.18)$$

where $y_{aa}^{\phi(S)}$ and $y_{aa}^{h_{\text{SM}}(S)}$ are given in Eqs. (2.13) and (2.11). The loop functions are F_1

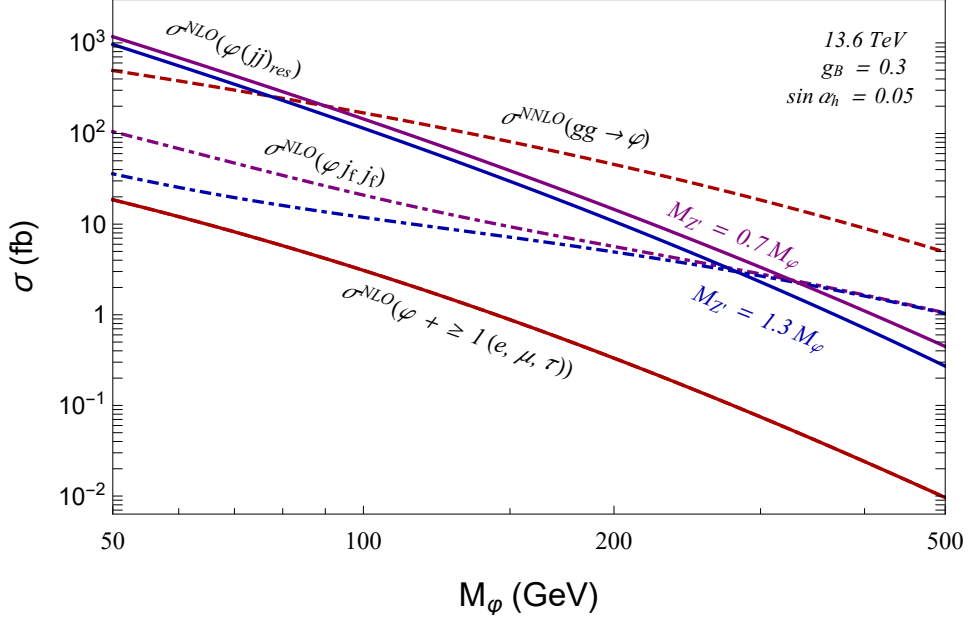


Figure 9: Cross sections at the 13.6 TeV LHC for φ production through gluon fusion (dot-dashed line), in association with a Z' (solid lines), and through Z' fusion (dashed lines), as a function of the φ mass. The displayed gluon fusion rate is calculated with MCFM [41,42] rescaled by the square of the mixing $\sin \alpha_h = 0.05$. The $Z'\varphi$ and φjj cross sections are computed at NLO in α_s for $M_{Z'}/M_\varphi = 0.7$ (upper lines) and 1.3 (lower lines), for a Z' gauge coupling $g_B = 0.3$; the cross section scales as g_B^4 for $Z'\varphi$ production, and as g_B^8 for Z' fusion.

defined in (2.24), and

$$F_V(x) = -2 - \frac{3}{x} + \frac{3}{x^2}(1 - 2x)Z(x) \quad (3.19)$$

with $Z(x)$ given in (2.25). In the minimal model, the sum runs over fields E_1 and E_2 . The strength of the $\gamma\gamma$ decay depends sensitively on the possible cancellation between the SM W and t loops and the charged anomalous, mainly governed by the magnitude of α_h and v' . The anomalous in the loop coherently add to the SM t , but destructively interfere with the SM W , resulting in a decrease of the overall strength of the diphoton decay. Furthermore, the anomalon contribution is controlled by the general Yukawa couplings y^ϕ from Eq. (2.11), including also the fermion mixing angles. The new 1-loop decays into $Z'\gamma$ and $Z\gamma$, with contributions from the anomalous which are again not suppressed by

mixing, are

$$\Gamma(\varphi \rightarrow Z'\gamma) = \frac{\alpha M_\varphi^3}{128\pi^4} \left(1 - \frac{M_{Z'}^2}{M_\varphi^2}\right)^3 \left| \cos \alpha_h \sum_{a,b=1}^2 \left(\frac{-2c_{ab}^{(Z')}}{M_a}\right) F^{V\gamma}(M_\varphi, M_{Z'}, M_a, M_b) + \sin \alpha_h \frac{g_B}{3v_h} F_2\left(\frac{4M_t^2}{M_\varphi^2}, \frac{4M_t^2}{M_{Z'}^2}\right) \right|^2, \quad (3.20)$$

and

$$\Gamma(\varphi \rightarrow Z\gamma) = \frac{\alpha M_\varphi^3}{128\pi^4} \left(1 - \frac{M_Z^2}{M_\varphi^2}\right)^3 \left| \cos \alpha_h \sum_{a,b=1}^2 \left(\frac{-2c_{ab}^{(Z)}}{M_a}\right) F^{V\gamma}(M_\varphi, M_Z, M_a, M_b) + \sin \alpha_h \frac{g}{v_h} \left[\frac{3 - 8s_W^2}{3c_W} F_2\left(\frac{4M_t^2}{M_\varphi^2}, \frac{4M_t^2}{M_Z^2}\right) + \frac{1}{2} F_{V2}\left(\frac{4M_W^2}{M_\varphi^2}, \frac{4M_W^2}{M_Z^2}\right) \right] \right|^2, \quad (3.21)$$

where $c_{ab}^{(Z')}$ and $c_{ab}^{(Z)}$ are the coupling structures given by (2.27), and

$$F_{V2}(x, y) = c_W \left[4 \left(3 - \frac{s_W^2}{c_W}\right) I_2(x, y) + \left(\left(1 + \frac{2}{x}\right) \frac{s_W^2}{c_W^2} - \left(5 + \frac{2}{x}\right) \right) I_1(x, y) \right], \quad (3.22)$$

with

$$I_1(x, y) = \frac{xy}{2(x-y)} + \frac{x^2y^2}{2(x-y)^2} (Z(1/x) - Z(1/y)) + \frac{x^2y}{(x-y)^2} (g(1/x) - g(1/y)), \quad (3.23)$$

$$I_2(x, y) = -\frac{xy}{2(x-y)} (Z(1/x) - Z(1/y)), \quad (3.24)$$

where $Z(x)$ and $g(x)$ are defined in (2.25) and (2.30), respectively. We note that $F_2(x, y) = I_1(x, y) - I_2(x, y)$ from (2.29), (3.23), and (3.24), consistent with [33]. For the $\varphi \rightarrow Z\gamma$ width, the anomalon and SM W loops add together and are partially canceled by the SM t , in contrast to $\varphi \rightarrow \gamma\gamma$, due to the corresponding electric charges.

The rich variety of exotic and SM-like decay channels for φ are shown in Figures 10 and 11. For the mixing-induced decays to two SM fermions, we include running of the respective Yukawa couplings using RunDec [43]. For the φ mass range shown, the nominally leading decay, $\varphi \rightarrow Z'Z'^*$, is actually a 3-body process and becomes kinematically suppressed for lighter M_φ . Hence, the mixing-angle induced SM-like Higgs decay modes compete with and are of the same order as the intrinsic φ decays. Notably, the $\varphi \rightarrow \gamma\gamma$ branching fraction is large, reflecting the anomalon-induced contribution and the interference with the SM loops. Similarly, the $Z'\gamma$ and $Z\gamma$ branching fractions also exhibit

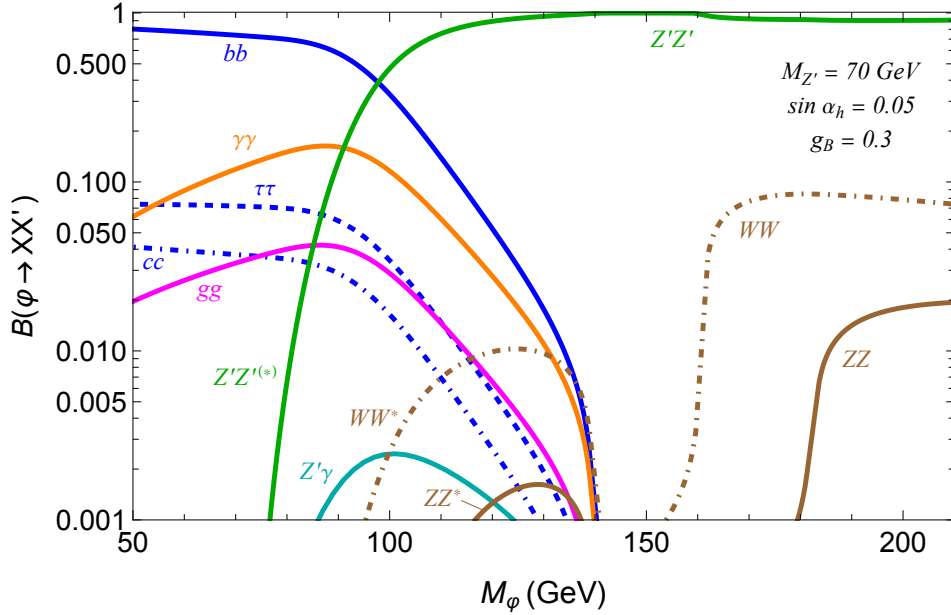


Figure 10: Branching fractions for the $U(1)_B$ -breaking scalar φ , as a function of its mass. The parameters fixed here are $\sin \alpha_h = 0.05$, $g_B = 0.3$, and $M_{Z'} = 70$ GeV. For the loop decays $\varphi \rightarrow \gamma\gamma$, $Z'\gamma$, we set the anomalon masses to 200 GeV and 250 GeV, and the anomalon mixing angles are $\theta = 0.3$ and $\chi = 0.25$.

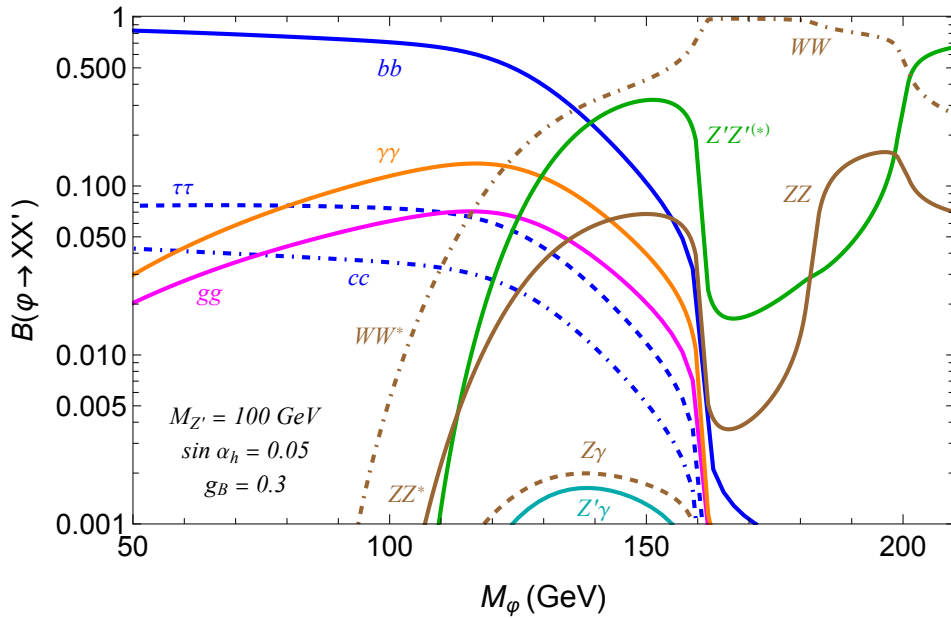


Figure 11: Branching fractions for φ as a function of M_φ , with all the parameters fixed as in Figure 10 except for $M_{Z'} = 100$ GeV.

different patterns compared to the simplest models of SM gauge singlets scalars. In general, determining the decay patterns of φ will give a complete picture of the underlying $U(1)_B$ charges of the decay products. For M_φ lighter than $M_{Z'}$, the two-body loop-induced $\gamma\gamma$ decay dominates over the four-body $\varphi \rightarrow Z'^*Z'^* \rightarrow 4j$ decay.

All tree level decays into SM quarks and leptons are suppressed by $\sin \alpha_h$, with the largest contribution coming from the decay into two bottom quarks. Additionally, the loop-suppressed gluon decay is also $\sin \alpha_h$ suppressed, in contrast to [16], since the anomalous are all colorless. For small α_h , the diphoton decay becomes the leading decay channel, justifying potential searches of φ in the diphoton spectrum. For larger M_φ , the phase space for decays into Z' and W/Z open up. Here, again, the tree-level decays into SM gauge bosons are suppressed by the Higgs mixing angle, although this can dominate over the $Z'Z'^*$ decay if the Z' mass is larger than the SM electroweak gauge boson masses. For example, with $M_{Z'} = 100$ GeV, the φ dominantly decays to SM gauge bosons for the mass range $160 \lesssim M_\varphi \lesssim 200$ GeV. For M_φ above twice the Z' mass, the $Z'Z'$ decay dominates. For scalar masses above twice the anomalon masses, the tree-level decay of φ into two anomalons is allowed, which dominates similar to the tree-level decays into vectorlike quarks in [16].

The leading constraint on the φ scalar comes from searches for a Higgs-like scalar in the diphoton decay channel, which is intrinsic to both unmixed scalars, ϕ and h_{SM}^0 . From Figure 4, for masses below $M_{Z'}$, ϕ dominantly decays to two photons. Hence, even though the introduction of a finite scalar mixing angle α_h with the SM Higgs boson leads to new two-body final states such as $b\bar{b}$, the interference of the diphoton channel for φ generally leads to sizeable $\varphi \rightarrow \gamma\gamma$ branching fractions, of the order of 10% or larger, even until the $2M_{Z'}$ threshold. As the diphoton decay enjoys a favorable signal to background ratio for the SM Higgs discovery in the light Higgs mass region, the considerations of an enhanced diphoton branching fraction and good signal to background ratio support our claim that the dominant constraint on the φ scalar arises from reinterpreting diphoton resonance searches.

Figure 12 shows the current ATLAS and CMS limits on $R_{\gamma\gamma}$ as a function of M_φ , where $R_{\gamma\gamma}$ is the ratio of the signal diphoton cross section to a SM Higgs diphoton cross section at the given M_φ mass (Additional limits at lower scalar masses are also performed in [44]). We also show the model prediction for $R_{\gamma\gamma}$ for three choices of $\sin \alpha_h = 0.1, 0.05,$ and 0.03 . Importantly, the diphoton signal strength shows a nontrivial scaling dependence on $\sin \alpha_h$: in particular, for $\sin \alpha_h = 0.1$ and $\sin \alpha_h = 0.05$, the $R_{\gamma\gamma}$ expectation is nearly

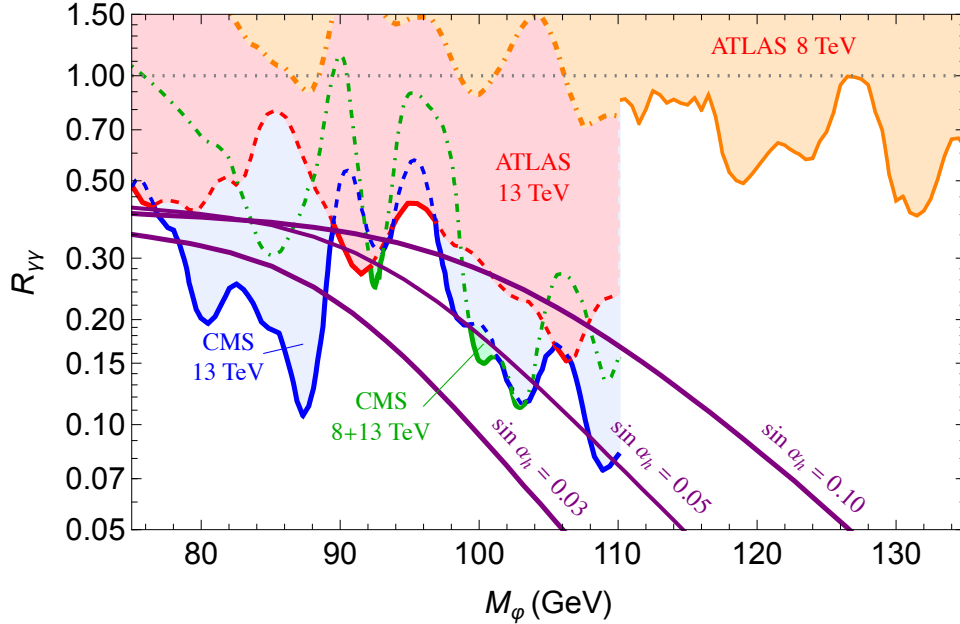


Figure 12: Predicted $R_{\gamma\gamma} \equiv \sigma(\phi \rightarrow \gamma\gamma)/\sigma(H \rightarrow \gamma\gamma)_{\text{SM}}$ as a function of M_ϕ for $g_B = 0.3$, $M_{Z'} = 70$ GeV, and $\sin \alpha_h = 0.1, 0.05$ or 0.03 (purple lines). We set the anomalon masses to 200 GeV and 250 GeV, and the anomalon mixing angles are $\theta = 0.3$ and $\chi = 0.25$. The shaded regions are excluded by CMS [45] and ATLAS [46, 47] diphoton resonance searches.

the same for $80 < M_\phi < 95$ GeV. This is because of two competing effects. First, as we increase α_h , the production rate from gluon fusion increases as $\sin^2 \alpha_h$. On the other hand, the interference between the SM Higgs and the ϕ diphoton decay processes is destructive, because the dominant mediator for SM Higgs to $\gamma\gamma$ is the W -boson, while the dominant mediators for ϕ to $\gamma\gamma$ are the charged anomalons, and there is a relative sign in their respective loop functions. This nontrivial scaling is a key aspect of our $Z' + \text{scalar}$ model, since the interference of the Higgs and exotic scalar diphoton decays will be a generic feature in chiral gauge extensions of the SM.

We now briefly highlight the differences between the latest experimental analyses and their corresponding sensitivities, as seen in Figure 12. In [45] by the CMS collaboration, the kinematic constraints on the transverse momenta are $p_T^{\gamma^1} = 30$ GeV and $p_T^{\gamma^2} = 18$ GeV, as well as $p_T^{\gamma^1}/M_{\gamma\gamma} = 0.47$ and $p_T^{\gamma^2}/M_{\gamma\gamma} = 0.28$, where 1 and 2 label the photon candidates with highest and second-highest transverse momentum and $M_{\gamma\gamma}$ is the invariant mass of the diphoton system. A portion of the early dataset required both photon candidates to be contained within the electromagnetic calorimeter barrel region, $|\eta| < 1.48$,

but the remainder of the dataset includes photons covered by the endcap regions covering $1.48 < |\eta| < 3.0$. In [46] by the ATLAS collaboration, the transverse energy requirements are $E_T > 22$ GeV for both photon candidates and $E_T/m_{\gamma\gamma} > 22/58 \approx 0.38$, with $|\eta| < 2.37$, excluding the transition region $1.37 < |\eta| < 1.52$. Both analyses use boosted decision trees to further optimize the signal selection against light jets faking photons and dielectron background events that appear similar to photons in the calorimeter. Further classifiers are used to characterize the production mode of the scalar resonance according to SM Higgs production expectations, dominantly targetting gluon fusion and vector boson fusion. Although the two analyses have comparable sensitivity to the φ diphoton signal, the improved acceptance of the diphoton system by CMS seems most responsible for their stronger exclusion contour, which goes down to $R_{\gamma\gamma} \simeq 0.07$ around $M_\varphi = 109$ GeV, while the best constraint from ATLAS is down to $R_{\gamma\gamma} \simeq 0.15$ for $M_\varphi = 106$ GeV.

We also show the earlier $\sqrt{s} = 8$ TeV analysis from ATLAS [47], which uses similar cuts as the newer exclusion papers as well as the Higgs discovery papers. We advocate new analyses that cover the diphoton invariant mass region above 110 GeV using current and future datasets. The possible overlap with the 125 GeV Higgs diphoton signal can be either masked with a narrow window, or more robustly, the mixing between the φ and the 125 GeV Higgs boson can be treated phenomenologically following the formalism in [39, 48, 49].

We remark that the existing constraints from diphoton searches can also be improved if a dedicated dijet + diphoton search is performed, given the expectation for Z' -associated production rates leading to an associated dijet resonance.

Interestingly, both experiments show an upward fluctuation in their $R_{\gamma\gamma}$ constraints for a diphoton resonance around 95 GeV, which could be explained by φ^1 . Namely, at 95.4 GeV, CMS observes a 2.9σ local (1.3σ global) excess [45] while ATLAS only observes a 1.7σ local significance [46]. In Figure 13, we show the contours of $R_{\gamma\gamma}$ as a function of g_B and $|\sin \alpha_h|$ for $M_\varphi = 95.4$ GeV and $M_{Z'} = 70$ GeV. The ATLAS and CMS measurements exclude $R_{\gamma\gamma} > 0.43$ and $R_{\gamma\gamma} > 0.57$, respectively. We also show the corresponding M_1 charged anomalon mass as vertical dot-dashed lines, and additional exclusions on $|\sin \alpha_h| > 0.24$ from (3.17) and $g_B > 0.52$ from Ref. [14]. We note that the $\tau\tau$ excess from CMS [50] requires an order one ratio between $\tau\tau$ and $\gamma\gamma$ widths, which cannot be accommodated in our model.

¹Related explanations can be found in [52].

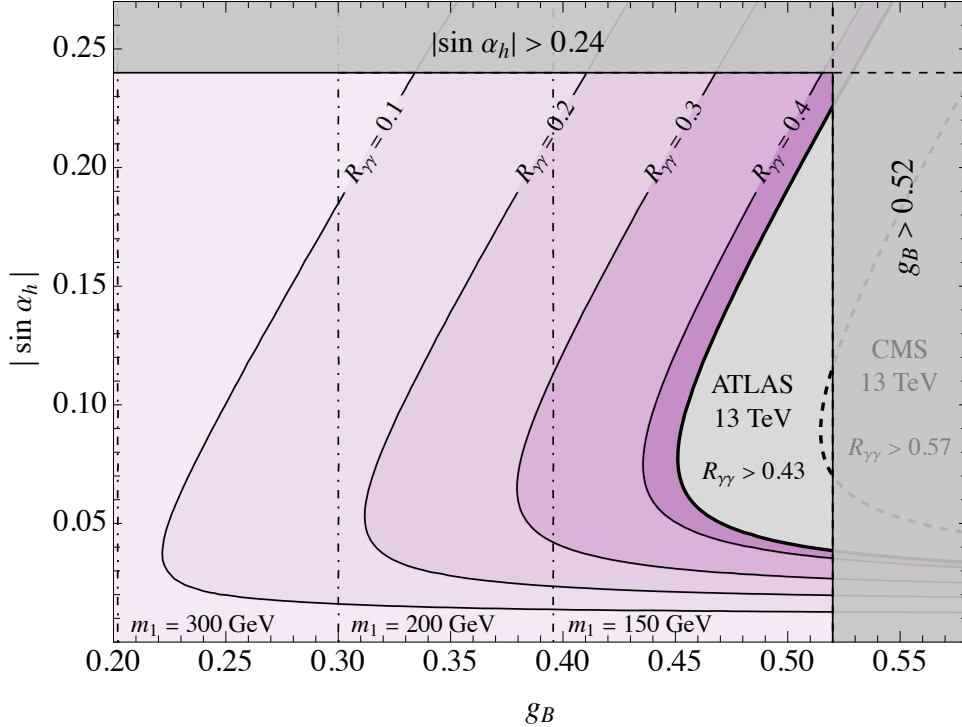


Figure 13: Contours of $R_{\gamma\gamma}$ for the φ diphoton signal as a function of g_B and $|\sin \alpha_h|$, with $M_\varphi = 95.4$ GeV and $M_{Z'} = 70$ GeV. The ATLAS constraint (solid black) of $R_{\gamma\gamma} < 0.43$ [46] and CMS constraint (dashed black) of $R_{\gamma\gamma} < 0.57$ [45] are also shown as gray regions. The vertical dot-dashed lines indicate the lighter m_1 charged anomalon mass. We also show the excluded region with $|\sin \alpha_h| > 0.24$ from the 125 GeV Higgs signal strength combination as well as $g_B > 0.52$ [14] from dijet resonance searches.

4 Conclusions

In this work, we have studied the phenomenology of the scalar ϕ associated with the spontaneous breaking of a $U(1)$ gauge symmetry beyond the SM. The generic mechanisms for ϕ production at hadron colliders, which only require $U(1)$ charges for light SM quarks, are in association with a Z' boson, or through Z' boson fusion (see diagrams in Figure 1). Our results for the cross sections of these processes at the LHC, computed at NLO, are shown in Figure 2.

If the SM quarks carry charges under the new $U(1)$, then the cancellation of the gauge anomalies typically requires the existence of new fermions (anomalons) with chiral charges under both the SM gauge groups and $U(1)$ symmetry. We emphasize that, like in the SM, the underlying chiral structure of the $U(1)$ symmetry is characterized by a single vev,

and hence the Z' , ϕ , and anomalon masses are unlikely to arbitrarily decouple from each other without violating perturbative unitarity.

The anomalons induce ϕ decays, at one loop, into $\gamma\gamma$, $Z'\gamma$, $Z\gamma$, ZZ , and WW , with the Z and W bosons being on- or off-shell depending on the ϕ mass. Another generic decay mode of ϕ , which occurs at tree level but may be highly phase-space suppressed, is into a pair of Z' bosons with one or both of them being off-shell depending on the mass ratio $M_\phi/M_{Z'}$.

In the presence of the portal coupling of ϕ to the SM Higgs doublet, the mass mixing between ϕ and h_{SM}^0 gives rise to a physical scalar, φ , in addition to the already discovered Higgs boson h^0 . This mixing induces additional φ decays (for example, $\varphi \rightarrow b\bar{b}, \tau^+\tau^-$) and production mechanisms (gluon fusion, associated φW , etc.). In addition, trilinear scalar interactions lead to $\varphi \rightarrow h^0 h^{0(*)}$ or $h^0 \rightarrow \varphi \varphi^{(*)}$, depending on the φ mass.

A particular challenging scenario to disentangle at colliders is that where the Z' is leptophobic, and the anomalons are heavier than $M_{Z'}/2$. To obtain a quantitative understanding of the various LHC signals in that scenario, we focused on the gauged quark-universal $U(1)_B$ symmetry, in which all SM quarks have the same coupling to the Z' . Furthermore, to compare the various scalar decay modes, we considered the minimal set of anomalons in Section 2, and showed that there is an interesting interplay between the $\phi \rightarrow Z'Z'^{(*)}$, $\gamma\gamma$, $Z'\gamma$, $Z\gamma$, ZZ and WW branching fractions (see Figure 4). Various aspects of the richer phenomenology of φ , in the presence of a sizable $\phi - h_{\text{SM}}^0$ mixing, are analyzed in Section 3.

Although the anomalons could be difficult to probe directly because of the electroweak production cross sections and model-dependent decays, the gauge singlet ϕ is promising since the anomalons mediate a nondecoupling diphoton decay. Hence, if the direct $\phi \rightarrow Z'Z'$ decay is kinematically forbidden and $\phi \rightarrow Z'jj$ is then suppressed by three-body phase space, the $\gamma\gamma$ and $Z'\gamma$ decays of ϕ are attractive discovery channels. When we include possible mixing with the SM Higgs field, the loop-induced decays gain additional impetus and can reveal new interference patterns of the underlying Yukawa couplings.

If both a Z' boson and a φ scalar will be discovered, there are many possible measurements to be made, including associated $Z'\varphi$ production and Z' fusion followed by several φ decay modes shown in Figures 10 and 11 (or in Figure 4 if the mixing with the SM Higgs is negligible). That set of measurements would elucidate the properties of the bosons and of the anomalons, as well as the new gauge structure.

Acknowledgments: This work is supported by the Cluster of Excellence *Precision Physics, Fundamental Interactions and Structure of Matter* (PRISMA⁺ – EXC 2118/1) within the German Excellence Strategy (project ID 390831469). LA and FY would like to thank the Theoretical Physics Division at Fermilab for their hospitality and support while the work was completed. Fermilab is administered by Fermi Forward Discovery Group, LLC under Contract No. 89243024CSC000002 with the U.S. Department of Energy, Office of Science, Office of High Energy Physics.

References

- [1] A. Pais, “Remark on baryon conservation,” *Phys. Rev. D* **8**, 1844-1846 (1973).
- [2] C. D. Carone and H. Murayama, “Possible light U(1) gauge boson coupled to baryon number,” *Phys. Rev. Lett.* **74**, 3122 (1995) [hep-ph/9411256].
- [3] D. C. Bailey and S. Davidson, “Is there a vector boson coupling to baryon number?,” *Phys. Lett. B* **348**, 185 (1995) [hep-ph/9411355].
- [4] C. D. Carone and H. Murayama, “Realistic models with a light U(1) gauge boson coupled to baryon number,” *Phys. Rev. D* **52**, 484 (1995) [hep-ph/9501220].
- [5] A. Aranda and C. D. Carone, “Limits on a light leptophobic gauge boson,” *Phys. Lett. B* **443**, 352 (1998) [hep-ph/9809522].
- [6] M. Carena, A. Daleo, B. A. Dobrescu and T. M. P. Tait, “ Z' gauge bosons at the Tevatron,” *Phys. Rev. D* **70**, 093009 (2004) [arXiv:hep-ph/0408098 [hep-ph]].
- [7] P. Fileviez Perez and M. B. Wise, “Breaking Local Baryon and Lepton Number at the TeV Scale,” *JHEP* **08**, 068 (2011) [arXiv:1106.0343 [hep-ph]].
- [8] M. Duerr, P. Fileviez Perez and M.B. Wise, “Gauge theory for baryon and lepton numbers with leptoquarks,” *Phys. Rev. Lett.* **110**, 231801 (2013) [arXiv:1304.0576].
- [9] B. A. Dobrescu and F. Yu, “Coupling-Mass Mapping of Dijet Peak Searches,” *Phys. Rev. D* **88**, no.3, 035021 (2013) [erratum: *Phys. Rev. D* **90**, no.7, 079901 (2014)] [arXiv:1306.2629 [hep-ph]].

- [10] B. A. Dobrescu and C. Frugiuele, “Hidden GeV-scale interactions of quarks,” *Phys. Rev. Lett.* **113**, 061801 (2014) [arXiv:1404.3947 [hep-ph]].
- [11] B. A. Dobrescu, “Leptophobic boson signals with leptons, jets and missing energy,” arXiv:1506.04435 [hep-ph].
- [12] B. A. Dobrescu, P. J. Fox and J. Kearney, “Higgs-photon resonances,” *Eur. Phys. J. C* **77**, no. 10, 704 (2017) [arXiv:1705.08433 [hep-ph]].
- [13] L. Michaels and F. Yu, “Probing new $U(1)$ gauge symmetries via exotic $Z \rightarrow Z'\gamma$ decays,” *JHEP* **03**, 120 (2021) [arXiv:2010.00021 [hep-ph]].
- [14] B. A. Dobrescu and F. Yu, “Dijet and electroweak limits on a Z' boson coupled to quarks,” *Phys. Rev. D* **109**, no.3, 3 (2024) [arXiv:2112.05392 [hep-ph]].
- [15] A. Kivel, J. Laux and F. Yu, “Axion couplings in gauged $U(1)$ ’ extensions of the Standard Model,” *JHEP* **03**, 078 (2023) [arXiv:2211.12155 [hep-ph]].
- [16] M. Duerr, P. Fileviez Perez and J. Smirnov, “Baryonic Higgs at the LHC,” *JHEP* **09**, 093 (2017) [arXiv:1704.03811 [hep-ph]].
- [17] M. A. Shifman, A. I. Vainshtein, M. B. Voloshin and V. I. Zakharov, “Low-Energy Theorems for Higgs Boson Couplings to Photons,” *Sov. J. Nucl. Phys.* **30**, 711-716 (1979) ITEP-42-1979.
- [18] K. Kumar, R. Vega-Morales and F. Yu, “Effects from New Colored States and the Higgs Portal on Gluon Fusion and Higgs Decays,” *Phys. Rev. D* **86**, 113002 (2012) [erratum: *Phys. Rev. D* **87**, no.11, 119903 (2013)] [arXiv:1205.4244 [hep-ph]].
- [19] A. Tumasyan *et al.* [CMS], “A portrait of the Higgs boson by the CMS experiment ten years after the discovery.,” *Nature* **607**, no.7917, 60-68 (2022) [erratum: *Nature* **623**, no.7985, E4 (2023)] [arXiv:2207.00043 [hep-ex]].
- [20] G. Aad *et al.* [ATLAS], “A detailed map of Higgs boson interactions by the ATLAS experiment ten years after the discovery,” *Nature* **607**, no.7917, 52-59 (2022) [erratum: *Nature* **612**, no.7941, E24 (2022)] [arXiv:2207.00092 [hep-ex]].
- [21] G. Aad *et al.* [ATLAS], “Characterising the Higgs boson with ATLAS data from Run 2 of the LHC,” *Phys. Rept.* **11**, 001 (2024) [arXiv:2404.05498 [hep-ex]].

- [22] J. Butterworth, H. Debnath, P. Fileviez Perez and Y. Yeh, “Dark matter from anomaly cancellation at the LHC,” *Phys. Rev. D* **110**, no.7, 075001 (2024) [arXiv:2405.03749 [hep-ph]].
- [23] J. Preskill, “Gauge anomalies in an effective field theory,” *Annals Phys.* **210**, 323-379 (1991).
- [24] T. Appelquist and M. S. Chanowitz, “Unitarity Bound on the Scale of Fermion Mass Generation,” *Phys. Rev. Lett.* **59**, 2405 (1987) [erratum: *Phys. Rev. Lett.* **60**, 1589 (1988)].
- [25] G. D. Kribs, G. Lee and A. Martin, “Effective field theory of Stückelberg vector bosons,” *Phys. Rev. D* **106**, no.5, 055020 (2022) [arXiv:2204.01755 [hep-ph]].
- [26] P. Fileviez Perez and M. B. Wise, “Baryon and lepton number as local gauge symmetries,” *Phys. Rev. D* **82**, 011901 (2010) [erratum: *Phys. Rev. D* **82**, 079901 (2010)] [arXiv:1002.1754 [hep-ph]].
- [27] E. Bernreuther and B. A. Dobrescu, “Vectorlike leptons and long-lived bosons at the LHC,” *JHEP* **07**, 079 (2023) [arXiv:2304.08509 [hep-ph]].
- [28] B. W. Lee, C. Quigg and H. B. Thacker, “Weak interactions at very high-energies: the role of the Higgs boson mass,” *Phys. Rev. D* **16**, 1519 (1977).
- [29] J. Alwall *et al.*, “The automated computation of tree-level and next-to-leading order differential cross sections, and their matching to parton shower simulations,” *JHEP* **1407**, 079 (2014) [arXiv:1405.0301 [hep-ph]].
- [30] A. Alloul, N. D. Christensen, C. Degrande, C. Duhr and B. Fuks, “FeynRules 2.0 - A complete toolbox for tree-level phenomenology,” *Comput. Phys. Commun.* **185**, 2250 (2014) [arXiv:1310.1921 [hep-ph]].
- [31] T. Hahn, “Generating Feynman diagrams and amplitudes with FeynArts 3,” *Comput. Phys. Commun.* **140**, 418 (2001) [hep-ph/0012260].
- [32] R. D. Ball *et al.* [NNPDF], “Parton distributions with QED corrections,” *Nucl. Phys. B* **877**, 290-320 (2013) [arXiv:1308.0598 [hep-ph]].
- [33] A. Djouadi, “The Anatomy of electro-weak symmetry breaking. I: The Higgs boson in the standard model,” *Phys. Rept.* **457**, 1 (2008) [hep-ph/0503172].

- [34] G. Passarino and M. J. G. Veltman, “One Loop Corrections for $e^+ e^-$ Annihilation Into $\mu^+ \mu^-$ in the Weinberg Model,” Nucl. Phys. B **160**, 151-207 (1979).
- [35] H. H. Patel, “Package-X: A Mathematica package for the analytic calculation of one-loop integrals,” Comput. Phys. Commun. **197**, 276 (2015) [arXiv:1503.01469]; “Package-X 2.0: A Mathematica package for the analytic calculation of one-loop integrals,” Comput. Phys. Commun. **218**, 66 (2017) [arXiv:1612.00009 [hep-ph]].
- [36] A. Tumasyan *et al.* [CMS], “Measurement of the Higgs boson inclusive and differential fiducial production cross sections in the diphoton decay channel with pp collisions at $\sqrt{s} = 13$ TeV,” JHEP **07**, 091 (2023) [arXiv:2208.12279 [hep-ex]].
- [37] G. Aad *et al.* [ATLAS], “Measurement of the $H \rightarrow \gamma\gamma$ and $H \rightarrow ZZ^* \rightarrow 4\ell$ cross-sections in pp collisions at $\sqrt{s} = 13.6$ TeV with the ATLAS detector,” Eur. Phys. J. C **84**, no.1, 78 (2024) [arXiv:2306.11379 [hep-ex]].
- [38] A. M. Sirunyan *et al.* [CMS], “Search for dark photons in Higgs boson production via vector boson fusion in proton-proton collisions at $\sqrt{s} = 13$ TeV,” JHEP **03**, 011 (2021) [arXiv:2009.14009 [hep-ex]].
- [39] P. Lo Chiatto and F. Yu, “Consistent electroweak phenomenology of a nearly degenerate Z' boson,” Phys. Rev. D **111**, no.3, 035001 (2025) [arXiv:2405.03396 [hep-ph]].
- [40] G. Aad *et al.* [ATLAS and CMS Collaborations], “Measurements of the Higgs boson production and decay rates and constraints on its couplings from a combined ATLAS and CMS analysis of the LHC pp collision data at $\sqrt{s} = 7$ and 8 TeV,” JHEP **1608**, 045 (2016) [arXiv:1606.02266 [hep-ex]].
- [41] R. Boughezal, J. M. Campbell, R. K. Ellis, C. Focke, W. Giele, X. Liu, F. Petriello and C. Williams, “Color singlet production at NNLO in MCFM,” Eur. Phys. J. C **77**, no.1, 7 (2017) [arXiv:1605.08011 [hep-ph]].
- [42] J. Campbell and T. Neumann, “Precision Phenomenology with MCFM,” JHEP **12**, 034 (2019) [arXiv:1909.09117 [hep-ph]].
- [43] K. G. Chetyrkin, J. H. Kuhn and M. Steinhauser, “RunDec: A Mathematica package for running and decoupling of the strong coupling and quark masses,” Comput. Phys. Commun. **133**, 43 (2000) [hep-ph/0004189].

- [44] G. Aad *et al.* [ATLAS], “Search for boosted diphoton resonances in the 10 to 70 GeV mass range using 138 fb^{-1} of 13 TeV pp collisions with the ATLAS detector,” JHEP **07**, 155 (2023) [arXiv:2211.04172 [hep-ex]].
- [45] A. Hayrapetyan *et al.* [CMS], “Search for a standard model-like Higgs boson in the mass range between 70 and 110 GeV in the diphoton final state in proton-proton collisions at $\sqrt{s} = 13 \text{ TeV}$,” Phys. Lett. B **860**, 139067 (2025) [arXiv:2405.18149].
- [46] G. Aad *et al.* [ATLAS], “Search for diphoton resonances in the 66 to 110 GeV mass range using pp collisions at $\sqrt{s} = 13 \text{ TeV}$ with the ATLAS detector,” JHEP **01**, 053 (2025) [arXiv:2407.07546 [hep-ex]].
- [47] G. Aad *et al.* [ATLAS Collaboration], “Search for scalar diphoton resonances in the mass range 65 – 600 GeV with the ATLAS detector in pp collision data at $\sqrt{s} = 8 \text{ TeV}$,” Phys. Rev. Lett. **113**, no. 17, 171801 (2014) [arXiv:1407.6583 [hep-ex]].
- [48] M. Frank, T. Hahn, S. Heinemeyer, W. Hollik, H. Rzehak and G. Weiglein, “The Higgs Boson Masses and Mixings of the Complex MSSM in the Feynman-Diagrammatic Approach,” JHEP **02**, 047 (2007) [arXiv:hep-ph/0611326 [hep-ph]].
- [49] E. Fuchs and G. Weiglein, “Breit-Wigner approximation for propagators of mixed unstable states,” JHEP **09**, 079 (2017) [arXiv:1610.06193 [hep-ph]]. D. Liu, J. Liu, C. E. M. Wagner and X. P. Wang, “A Light Higgs at the LHC and the B-Anomalies,” JHEP **1806**, 150 (2018) [arXiv:1805.01476 [hep-ph]]. R. Vega, R. Vega-Morales and K. Xie, “Light (and darkness) from a light hidden Higgs,” JHEP **1806**, 137 (2018) [arXiv:1805.01970 [hep-ph]].
- [50] A. Tumasyan *et al.* [CMS], “Searches for additional Higgs bosons and for vector leptoquarks in $\tau\tau$ final states in proton-proton collisions at $\sqrt{s} = 13 \text{ TeV}$,” JHEP **07**, 073 (2023) [arXiv:2208.02717 [hep-ex]].
- [51] P. Fileviez Perez, S. Ohmer and H. H. Patel, “Minimal Theory for Lepto-Baryons,” Phys. Lett. B **735**, 283-287 (2014) [arXiv:1403.8029 [hep-ph]].
- [52] P. J. Fox and N. Weiner, “Light Signals from a Lighter Higgs,” JHEP **08**, 025 (2018) [arXiv:1710.07649 [hep-ph]].